



Original article

Altered synaptic currents, mitophagy, mitochondrial dynamics in Alzheimer's disease models and therapeutic potential of Dengzhan Shengmai capsules intervention

Binbin Zhao ^{a, b, 1}, Dongfeng Wei ^{c, 1}, Qinghua Long ^d, Qingjie Chen ^e, Fushun Wang ^f, Linlin Chen ^g, Zefei Li ^b, Tong Li ^b, Tao Ma ^h, Wei Liu ⁱ, Linshuang Wang ^c, Caishui Yang ^{a, j}, Xiaxia Zhang ^{a, k}, Ping Wang ^{b, **}, Zhanjun Zhang ^{a, k, *}

^a State Key Laboratory of Cognitive Neuroscience and Learning & IDG/McGovern Institute for Brain Research, Beijing Normal University, Beijing, 100875, China

^b Institute of Gerontology, Hubei University of Chinese Medicine, Wuhan, 430065, China

^c Institute of Basic Research in Clinical Medicine, China Academy of Chinese Medical Sciences, Beijing, 100700, China

^d Medical School, Hubei Minzu University, Enshi, Hubei, 445000, China

^e HuBei University of Science and Technology, Xianning, Hubei, 437100, China

^f Institute of Brain and Psychological Science, Sichuan Normal University, Chengdu, 610066, China

^g Key Laboratory of Traditional Chinese Medicine Resource and Compound Prescription, Ministry of Education, Hubei University of Chinese Medicine, Wuhan, 430065, China

^h Dongfang Hospital, Beijing University of Chinese Medicine, Beijing, 100078, China

ⁱ Beijing Key Laboratory of Traditional Chinese Medicine Basic Research on Prevention and Treatment for Major Diseases, Experimental Research Center, China Academy of Chinese Medical Sciences, Beijing, 100700, China

^j School of Systems Science, Beijing Normal University, Beijing, 100875, China

^k BABRI Centre, Beijing Normal University, Beijing, 100875, China

ARTICLE INFO

Article history:

Received 14 June 2023

Received in revised form

25 September 2023

Accepted 19 October 2023

Available online 28 October 2023

Keywords:

Alzheimer's disease

Synaptic currents

Mitophagy

Mitochondrial fusion and fission

Dengzhan Shengmai capsules

ABSTRACT

Emerging research suggests a potential association of progression of Alzheimer's disease (AD) with alterations in synaptic currents and mitochondrial dynamics. However, the specific associations between these pathological changes remain unclear. In this study, we utilized A β ₄₂-induced AD rats and primary neural cells as *in vivo* and *in vitro* models. The investigations included behavioural tests, brain magnetic resonance imaging (MRI), liquid chromatography-tandem mass spectrometry (UPLC-MS/MS) analysis, Nissl staining, thioflavin-S staining, enzyme-linked immunosorbent assay, Golgi-Cox staining, transmission electron microscopy (TEM), immunofluorescence staining, proteomics, adenosine triphosphate (ATP) detection, mitochondrial membrane potential (MMP) and reactive oxygen species (ROS) assessment, mitochondrial morphology analysis, electrophysiological studies, Western blotting, and molecular docking. The results revealed changes in synaptic currents, mitophagy, and mitochondrial dynamics in the AD models. Remarkably, intervention with Dengzhan Shengmai (DZSM) capsules emerged as a pivotal element in this investigation. A β ₄₂-induced synaptic dysfunction was significantly mitigated by DZSM intervention, which notably amplified the frequency and amplitude of synaptic transmission. The cognitive impairment observed in AD rats was ameliorated and accompanied by robust protection against structural damage in key brain regions, including the hippocampal CA3, primary cingulate cortex, prelimbic system, and dysgranular insular cortex. DZSM intervention led to increased IDE levels, augmented long-term potential (LTP) amplitude, and enhanced dendritic spine density and length. Moreover, DZSM intervention led to favourable changes in mitochondrial parameters, including ROS expression, MMP and ATP contents, and mitochondrial morphology. In conclusion, our findings delved

Peer review under responsibility of Xi'an Jiaotong University.

* Corresponding author. State Key Laboratory of Cognitive Neuroscience and Learning & IDG/McGovern Institute for Brain Research, Beijing Normal University, Beijing, 100875, China.

** Corresponding author.

E-mail addresses: pwang54@aliyun.com (P. Wang), zhang_rzs@bnu.edu.cn (Z. Zhang).

¹ Both authors contributed equally to this work.

<https://doi.org/10.1016/j.jpha.2023.10.006>

2095-1779/© 2023 The Authors. Published by Elsevier B.V. on behalf of Xi'an Jiaotong University. This is an open access article under the CC BY-NC-ND license (<http://creativecommons.org/licenses/by-nc-nd/4.0/>).

into the realm of altered synaptic currents, mitophagy, and mitochondrial dynamics in AD, concurrently highlighting the therapeutic potential of DZSM intervention.

© 2023 The Authors. Published by Elsevier B.V. on behalf of Xi'an Jiaotong University. This is an open access article under the CC BY-NC-ND license (<http://creativecommons.org/licenses/by-nc-nd/4.0/>).

1. Introduction

Alzheimer's disease (AD) is a neurodegenerative disease with cognitive impairment as its core symptom. With the burgeoning in number of older individuals, the number of patients with AD in China is also increasing. An epidemiological survey reported that the number of patients with AD aged ≥ 60 years has exceeded 10 million in China [1]. The increased prevalence of AD imposes a heavy burden on the society and economy. A recent study predicted that the total expenditure required for management of AD in China will exceed US\$ 1.8 trillion by 2050 [2].

Synapses serve as crucial junctions for transmission of information between neurons. Changes in synaptic currents may lead to aberrant synaptic function, thereby disrupting normal communication between neurons. However, the specific link between alterations in synaptic currents and pathological changes observed in AD remains largely elusive, presenting numerous unresolved questions [3,4]. Perturbations in mitochondrial dynamics, including alterations in mitochondrial morphology, distribution, fusion, fission, and clearance, have been observed in AD [5,6]. Senile plaques (SPs) are formed through aggregation of β -amyloid ($A\beta$) proteins. On the other hand, neurofibrillary tangles (NFTs) are formed as a result of mitochondrial dysfunction, neuronal loss and synaptic dysfunction. Mitochondrial dysfunction is an important pathological change in AD, which primarily manifests as mitochondrial ultrastructural damage, decreased adenosine triphosphate (ATP) levels, increased reactive oxygen species (ROS) levels, and reduced mitochondrial membrane potential (MMP) [7,8]. However, existing drugs only improve AD symptoms and do not fundamentally prevent or reverse the pathological progression of AD. Therefore, prevention and treatment of AD has become an increasingly serious issue, and more effective treatment methods and drugs are urgently needed.

Mitochondria are important organelles, which mainly provide energy to cells, and regulate calcium/iron homeostasis and apoptosis [9,10]. Neurons are highly differentiated mitotic cells that have a high demand for bioenergy. The structure and function of neurons are inherently dependent on the mitochondria. However, the structure and function of mitochondria get impaired due to aging, which ultimately triggers mitochondrial dysfunction [11,12]. Several studies have demonstrated that mitochondrial dysfunction is an important pathophysiological change that occurs in patients with AD. Mitochondrial dysfunction may occur in the early stage of AD, even before the formation of SPs and NFTs [13–15]. Mitochondrial dysfunction mainly manifests as mitochondrial ultrastructural damage, decreased ATP levels, increased ROS levels, and reduced MMP. Under physiological conditions, mitochondrial morphology and function are strictly controlled and regulated by the core pathways, including mitochondrial biogenesis, mitophagy, and mitochondrial fusion/fission imbalance [16,17]. Patients with AD show defects in mitophagy and an imbalance between mitochondrial fusion and fission. Improvement in mitophagy and mitochondrial fusion/fission have been reported to significantly alleviate mitochondrial dysfunction and synaptic disorder in patients with AD, and ultimately relieve cognitive impairment [18–20]. Therefore, regulation of mitophagy and mitochondrial fusion/fission is an effective strategy for delaying the pathological processes of AD.

Dengzhan Shengmai (DZSM) capsules are traditional Chinese medicinal compounds. It consists of dried whole herb of *Erigeron brevisca pus* (Vant.) Hand.-Mazz. (Family: Asteraceae Bercht. and J. Presl, Dengzhanxixin in Chinese), dried roots or rhizomes of *Panax ginseng* CA Mey (Family: Araliaceae, Renshen in Chinese), dried tuberous roots of *Ophiopogon japonicus* (L.f.) Ker-Gawl. (Family: Liliaceae, Maidong in Chinese), and dried ripe fruits of *Schisandra chinensis* (Turcz.) Baill. (Family: Magnoliaceae Juss., Wuweizi in Chinese). DZSM was approved for marketing by the China National Medical Products Administration (NMPA) in 2007. Since then, it has been widely used to treat a variety of central nervous system diseases, including AD, chronic cerebral ischemia, and vascular cognitive impairment (VCI) [21–23]. In addition, DZSM was also included in China's National Essential Medicine List in 2018. Our previous studies have demonstrated that DZSM alleviates cognitive impairment in patients with AD and amyloid precursor protein (APP)/presenilin 1 (PS1) mice. Moreover, it also inhibits $A\beta$ deposition in the hippocampus of APP/PS1 mice by reducing the levels of soluble $A\beta_{40}$ and $A\beta_{42}$ [21,22]. Previous studies have also shown that DZSM and its active components inhibit neuroinflammation and oxidative stress, and improve synaptic disorders in neurodegenerative diseases [24,25].

Based on the findings of the previous research by our group and the aforementioned research background, the aim of this study was to delve into the investigation of altered synaptic currents, mitophagy, and mitochondrial dynamics in AD models to uncover the underlying molecular mechanisms that drive cognitive impact, neuronal loss mitigation, and synaptic dysfunction. This study also focused on exploring the therapeutic potential of DZSM as an intervention against AD-related changes. These two facets are intricately interwoven and collectively form the basis of our study.

2. Materials and methods

2.1. Animals

A total of 60 specific pathogen-free (SPF) grade male Sprague Dawley (SD) rats, weighing (200 ± 20) g, were purchased from Changsheng Biotechnology Co., Ltd. (Benxi, China) (Permit number: SYXK (Liao) 2020–0001). The rats were housed at the Experimental Animal Centre of the Hubei University of Traditional Chinese Medicine. The temperature in the animal room was controlled to range between 23°C and 25 °C, and the relative humidity was maintained at 40%–50%. During the experimental period, rats were allowed free access to food and water. This study was approved by the Animal Ethics Committee of the Hubei University of Traditional Chinese Medicine (Approval number: HUCMS 00267195), and all the experimental procedures were performed in accordance with the regulations of the Animal Ethics Committee.

2.2. Materials and instruments

DZSM was purchased from Yunnan Biovalley Pharmaceutical Co., Ltd. (0.18 g/capsule, batch number: 20180655; Kunming, China). $A\beta_{1-42}$ polypeptide (cat: A9810) was obtained from Sigma (St. Louis, MO, USA). Trypsin (T1360), CCK8 kit (cat: CA1210), ATP detection kit (cat: BC0300), MMP Assay Kit with JC-1 (M8650), ROS assay kit (cat: CA1410), and BCA protein assay kit (cat: PC0020)

were purchased from Solarbio Science & Technology (Beijing, China). Enzyme-linked immunosorbent assay (ELISA) kits, including AMP ELISA (cat: DRE08741) and ATP ELISA (cat: DRE08527), were purchased from Lian Shuo Biotechnology (Shanghai, China). A β_{40} ELISA (cat: E-EL-R3030) and A β_{42} ELISA (cat: E-EL-R1402c) were purchased from Elabscience (Wuhan, China). Cy3-labelled (cat: GB21303) and FITC-labelled goat anti-rabbit secondary antibodies (cat: GB21303) were purchased from Servicebio Technology Co., Ltd. (Wuhan, China). The fluorescence microscope (Nikon Eclipse C1) was purchased from Nikon (Tokyo, Japan). The polyvinylidene fluoride (PVDF) membranes (IPVH00010) were purchased from Immobilon (Darmstadt, Germany). The gel imaging and analysis system (WD-9413A) was obtained from Liuyi Biotechnology (Beijing, China). The FD Rapid GolgiStain Kit (cat: PK401) was purchased from FD NeuroTechnologies (Colombia, MD, USA).

A stereotaxic apparatus (model 51,700) was purchased from Stoelting (Wood Dale, IL, USA). Morris water maze (MWM, Version 2.0) was purchased from Zhenghua Biologic Apparatus Facilities (Huaibei, China). The new object recognition (NOR) apparatus (EthoVision XT, Version 15.0) was purchased from Noldus Information Technology (Wageningen, Netherlands). The FMRIB software library (FSL, version 6.0.2) was created by the Analysis Group (Oxford, UK). An Agilent 6460 Triple Quadrupole Mass Spectrometer was purchased from Agilent Technologies (Santa Clara, CA, USA). The microtome (RM2016) was obtained from Leica (Wetzlar, Germany). An upright educational microscope (Nikon Eclipse E100) and a fluorescence microscope (Nikon Eclipse C1) were purchased from Nikon. A confocal laser-scanning microscope (OLS5100) was purchased from Olympus (Tokyo, Japan). Transmission electron microscope (HT-7800) was purchased from Hitachi (Tokyo, Japan). Reverse-phase column chromatography was purchased from Waters OASIS (Milford, MA, USA). MitoTracker Red CMXRos (M9940) was purchased from Solarbio Science & Technology Co., Ltd. (Beijing, China).

2.3. Groups and intracerebroventricular (ICV) injection of A β_{1-42}

After one week of adaptive feeding, the rats were divided into four groups using a random number table: control group (sham-operated), DZSM group, AD group, and AD + DZSM group. Each group comprised 15 rats. AD models were established by administering intracerebroventricular injection of A β_{1-42} to the rats in accordance with the method described by Zhang et al. [26] and our previous studies [27]. Briefly, A β_{1-42} polypeptide was dissolved in dimethyl sulfoxide (DMSO), diluted with sterile normal saline to a concentration of 2.6 $\mu\text{g}/\mu\text{L}$, and incubated at 37 °C for one week. The rats were immobilised on a stereotaxic apparatus after administering deep anaesthesia with a mixture of ketamine (100 mg/kg) and dexmedetomidine (0.5 mg/kg). Using a stereotaxic map, a small hole (depth, 4.0 mm; diameter, 1 mm) was drilled 0.9 mm behind the fontanelle and 1.5 mm left/right of the sagittal line (AP = 0.9, L = 1.5, V = 4.0). The prepared A β_{1-42} polypeptide (2.5 μL) was injected bilaterally into the ventricles of the rat using a microinjector. The injection was administered at a speed of 0.5 $\mu\text{L}/\text{min}$. After the surgery, penicillin (100,000 U/i.m.) was injected intraperitoneally to each rat for three consecutive days to prevent infection.

2.4. Drugs and treatment

DZSM comprises dried whole herb of *Erigeron breviscapus* (Vant.) Hand.-Mazz. (Family: Asteraceae Bercht. & J. Presl, Dengzhanxixin in Chinese), dried roots or rhizomes of *Panax ginseng* CA

Mey (Family: Araliaceae, Renshen in Chinese), dried tuberous roots of *Ophiopogon japonicus* (L. f) Ker-Gawl (Family: Liliaceae, Maidong in Chinese), and dried ripe fruits of *Schisandra chinensis* (Turcz.) Baill. (Family: Magnoliaceae Juss., Wuweizi in Chinese). The dose was determined on the basis of the equivalent dose ratio between humans and animals in terms of body surface area and clinical equivalent dose. The DZSM and AD + DZSM groups were administered DZSM intragastrically at a dose of 100 mg/kg/day, whereas the control and AD groups received normal saline (10 mL/kg/day) via gavage. All groups were gavaged once per day for four consecutive weeks. A schematic illustration of the study design and timeline are shown in Fig. 1A.

2.5. Preparation of blank serum and DZSM-containing serum/cerebrospinal fluid (CSF)

Ten SD rats were selected and randomly divided into a blank group and a DZSM group (five rats in each group). After adaptive feeding, the rats were gavaged with normal saline and DZSM. The DZSM group was gavaged with an appropriate dose of DZSM, while the blank group was gavaged with an equivalent volume of normal saline. All groups were gavaged three times per day for seven consecutive days. Two hours after the last gavage, the rats were anaesthetised with a mixture of ketamine (100 mg/kg) and dexmedetomidine (0.5 mg/kg). Blood samples were acquired by puncturing the abdominal aorta. Serum and CSF were subsequently collected and preserved at –80 °C until processing.

2.6. Cell culture and treatment

2.6.1. Preparation and culture of primary neural cells

Primary neural cells were obtained in accordance with the methods reported in the literature [28,29]. Briefly, embryonic mice (C57BL/6) were selected at 17.5 days of gestation (E17.5). Brain tissue was isolated and dissected using Hank's balanced salt solution (HBSS), which was then incubated with 0.25% trypsin (T1360) for 15 min at room temperature, and then centrifuged at 1,000 g for 5 min. The supernatants were collected. Subsequently, DME/F12 medium (containing 10% fetal bovine serum (FBS)) was added, and centrifugation was performed (1,000 g, 5 min) to obtain primary neural cells. The cells were seeded onto cell culture plates and cultured at 37 °C in an atmosphere containing 5% carbon dioxide. After 4–8 days of cultivation, the culture medium was discarded and replaced with fresh DME/F12 medium (containing 10% FBS). Thereafter, half of the medium was replaced every three days until further treatment.

2.6.2. Treatment of primary neural cells

A β_{1-42} solution (5 mM) was prepared by dissolving A β_{1-42} polypeptide in DMSO, with further dilution using phosphate-buffered saline (PBS) to obtain various concentrations (0.01, 0.1, 1, 2, 5, and 10 μM). The A β_{1-42} solutions were incubated at 4 °C for 24 h. Subsequently, various concentrations of A β_{1-42} solution were added to primary neural cells in the logarithmic growth stage and incubated for 6, 12, 24 and 48 h. To determine the optimal A β_{42} concentration required to damage primary neural cells, cell viability was examined using a CCK8 kit. Primary neural cells in the logarithmic growth stage were incubated in different concentrations of DZSM-containing serum (5%, 10%, 20%, and 40%) for 6, 12, 24, and 48 h. Cell viability was assessed using a CCK8 kit, the results of which allowed the determination of optimal concentration of DZSM-containing serum for protection of primary neural cells. In this study, 10 μM A β_{1-42} and 10% DZSM-containing serum were ultimately selected for the experiments, and the length of

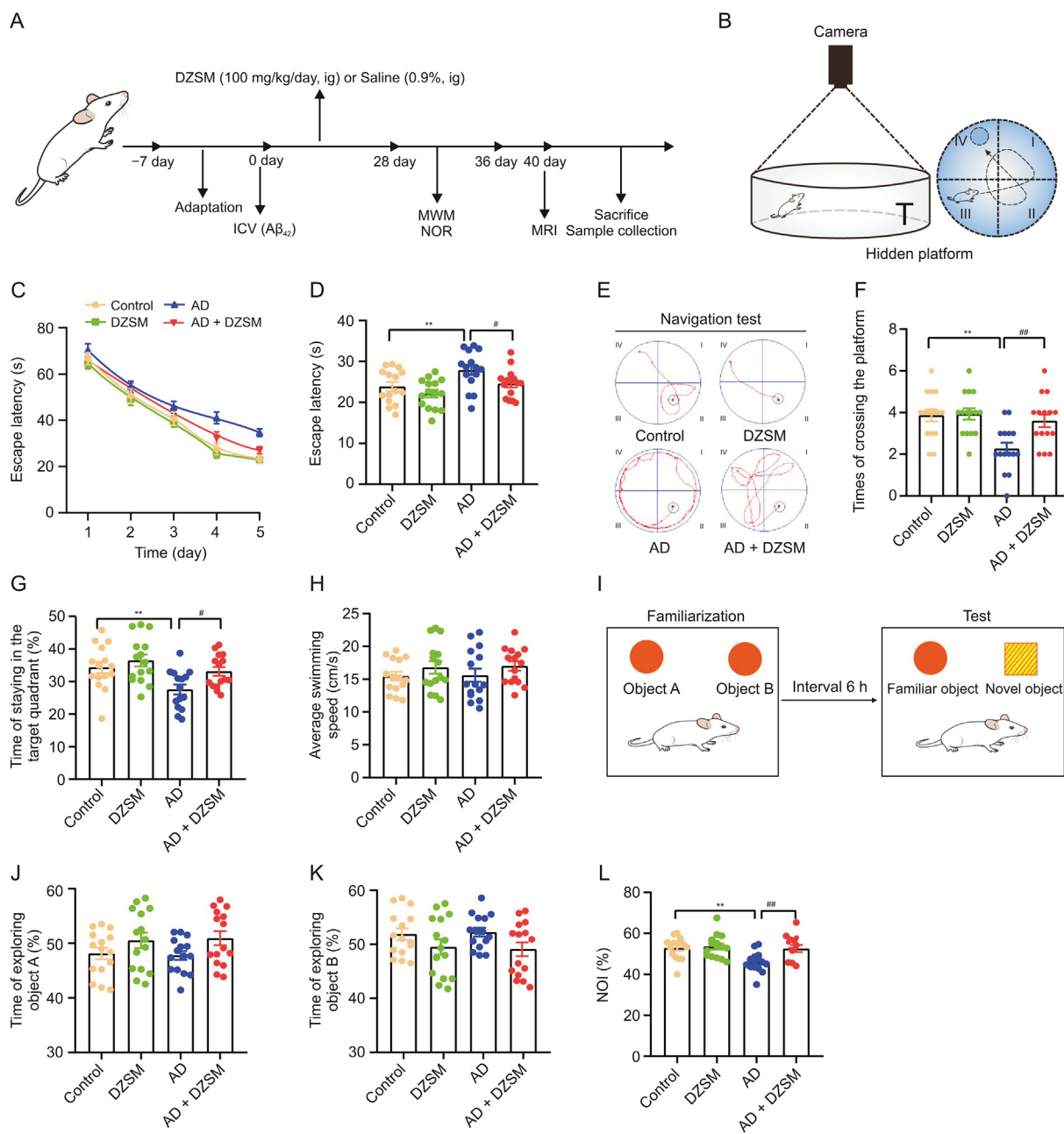


Fig. 1. Dengzhan Shengmai (DZSM) improves $A\beta_{42}$ -induced cognitive impairment in rats. (A) The schematic illustration of the study design and timeline. (B) Schematic diagram of the Morris water maze (MWM) test. (C) Line chart of the changes in escape latency during the training period. (D) Statistical histogram of escape latency on the day 5. (E) Representative trajectory chart of the place navigation test. (F) Statistical histogram showing the times of crossing the platform in the spatial probe test. (G) Statistical histogram showing the time within the target quadrant in the spatial probe test. (H) Statistical histogram of the average swimming speed in the spatial probe test. (I) Schematic diagram of the new object recognition test. (J) Comparison plot of the amount of time that rats spent exploring object A during the familiarization period. (K) Comparison plot of the amount of time rats spent exploring object B during the familiarization period. (L) Statistical histogram of the new-object recognition index (NOI) during the test period. Experimental data are expressed as the mean \pm standard error of mean (SEM), $n = 15$. ** $P < 0.01$ vs. Control group, and # $P < 0.05$ and ## $P < 0.01$ vs. AD group. AD: Alzheimer’s disease; ICV: intra-cerebroventricular; MRI: magnetic resonance imaging; NOR: new object recognition.

treatment was determined to be 24 h. Primary neural cells were divided into: control, $A\beta_{42}$, $A\beta_{42} + DZSM$, and $A\beta_{42} +$ mitochondrial division inhibitor 1 (Mdivi1) groups. The control and $A\beta_{42}$ groups were treated with blank serum and $10 \mu M A\beta_{42}$, respectively, for 24 h. The $A\beta_{42} + DZSM$ and $A\beta_{42} + Mdivi1$ groups were pre-treated with $10 \mu M A\beta_{42}$ for 2 h, followed by 24 h of treatment with 5% DZSM-containing serum and $5 \mu M Mdivi1$ (purity $\geq 98\%$, M0199, Sigma-Aldrich, St. Louis, MO, USA), respectively.

2.7. Behavioural tests

The MWM and NOR tests are behavioural detection methods used to evaluate learning and memory in rodents [30]. These tests have been widely used to examine cognitive function in neurodegenerative diseases, including AD and Parkinson’s disease (PD). The MWM and NOR tests were used to evaluate the cognitive function in various groups of rats.

2.7.1. NOR test

The NOR apparatus consisted of an experimental box (length 50 cm × width 50 cm × height 50 cm) along with a behavioural tracking and analysis system. During the familiarization period, two identical objects were placed in the experimental box (marked as objects A and B). The rats were transferred from the non-object area to the experimental box, and the behaviour tracking and analysis system recorded the amount of time spent by the rats exploring the objects in a duration of 5 min. The test period started after an interval of 6 h. First, one of the objects in the experimental box was replaced with a new object composed of the same material, but different colour and shape (marked as the novel object), whereas the other object was retained (marked as the familiar object). The rats were placed in the experimental box, and the behavioural tracking and analysis system recorded the amount of time the rats spent exploring the new/old objects in a duration of 5 min. The time spent exploring objects A/B during the familiarization period and the new-object recognition index (NOI) during the test period were calculated and analysed using the following formula:

$$\text{NOI} = \frac{\text{time spent exploring the novel object}}{(\text{time spent exploring the novel object} + \text{time spent exploring the familiar object})} \times 100\%.$$

2.7.2. MWM test

To evaluate whether DZSM alleviated the learning/memory impairment induced by $A\beta_{42}$, the MWM test was performed to examine the learning-memory ability of rats. The MWM used in this study consisted of a circular pool (diameter 150 cm × height 60 cm), a circular platform (diameter 12 cm × height 35 cm) and a video analysis system. The MWM test consisted of place navigation and spatial probe tests. The place navigation test evaluated the memory ability of the rats via escape latency, and the spatial probe test evaluated the learning ability of the rats based on the times of crossing the platform and the amount of time spent on the original platform. Briefly, the training period commenced on day 1 and ended on day 5. The rats were trained four times per day, and each training session lasted 90 s. If the rat failed to find the platform within 90 s, it was guided to the platform and allowed to stay there for 15 s. After one day of rest, the rats were subjected to place navigation test. The video analysis system recorded the escape latency and swimming trajectory of the rats. On the 7th day, the circular platform was removed and the spatial probe test was conducted. The video analysis system recorded the times of crossing the platform and the time spent in target quadrant within a duration of 90 s.

2.8. Imaging and examination

2.8.1. Brain MRI examination

The rats were subjected to MRI at the baseline and on the 40th day after drug treatment. The animals were anaesthetised with isoflurane (mixed in pure oxygen at concentrations of 1.5%–2%), which was delivered via a nose cone. The heart rate and respiration of the animals were continuously monitored during the imaging sessions. A total of 14 rats from the AD + DZSM group and 15 rats from the AD group were included. The MRIs were performed with a 7T/20-cm-diameter bore Bruker Biospec scanner at Capital Medical University. A volume coil was used for radiofrequency transmission and a quadrature surface coil was used for signal detection. T2-weighted images were acquired using the following RARE sequence: repetition time = 6300 ms, echo time = 24 ms, matrix size 256 × 256, and

scanning layer thickness = 0.3 mm. The imaged field of view (FOV) included the olfactory bulb, cerebellum, and extra-brain tissue. Diffusion tensor images were acquired using the following EPI sequence: repetition time = 6, 250 ms, echo time = 22 ms, b-value = 1000 s/mm², diffusion gradient pulse duration (δ) = 4.204 ms, diffusion gradient separation (Δ) = 14.665 ms, diffusion direction = 36, field of view = 3.0 × 3.0 cm², matrix size 128 × 128, slice = 25, scanning layer thickness = 0.8 mm, and resolution = 0.234375 × 0.234375 × 0.8 cm³.

2.8.2. Image data processing and statistical analyses of MRI

The acquired diffusion tensor imaging (DTI) data was first processed along with T2-weighted data via atlas normalization toolbox using Elastix 2 [31–33]. Image data in Bruker format were converted to neuroimaging informatics technology initiative (NIFTI) format and normalised to SIGMA space. After orientation examination, brain and brain structure masks were acquired by segmenting all the original structural images, and field non-uniformity correction was conducted to reduce the linear grey scale of the image caused by uneven surface coils. The acquired grey and white matter images of each rat were used to prepare the grey and white matter templates using DARTEL, which were subsequently registered to the DTI data using the FSL. MRtrix3 was used to preprocess the DTI data [34]. DTI data were denoised, and the bias field was corrected to remove noise and correct for B1 field nonuniformity [35]. Additionally, the voxel size was scaled up 10 times to apply the FSL eddy correction to correct distortions and motion artefacts [36]. The pre-processed data were converted to raw resolution and used to generate the diffusion tensor after removing negative values, including fractional anisotropy (FA) and mean diffusivity (MD). Voxel-based analysis was conducted by applying two-sample *t*-tests on diffusion tensor between the AD and AD + DZSM groups, and the results were further corrected for multiple comparisons and contemplated to be significant at corrected $P < 0.05$, with an uncorrected $P < 0.01$, and a cluster size larger than 146.

2.9. Analytical techniques

2.9.1. Sample preparation and serum pharmacochemical analysis using UPLC-MS/MS

Rat plasma or CSF (100 μ L) was loaded on a Waters Oasis HLB cartridge preconditioned with methanol and water, which was washed with 1.0 mL water, sucked dry, and eluted with 1.0 mL of methanol with the flow rate of 1 mL/min. The eluate was evaporated to dry under a gentle stream of nitrogen at 40 °C and the residue was reconstituted using 100 μ L methanol. After being centrifuged at 9,000 g, 5 μ L of the supernatant was injected into the UPLC-MS/MS system for analysis.

The UPLC-MS/MS analyses were performed using an Agilent 1290 Infinity series connected to an Agilent 6460 Triple Quadrupole Mass Spectrometer with an ESI source. Chromatographic separation was achieved on a Agilent ZORBAX RRHD Eclipse Plus C₁₈ column (100 mm × 2.1 mm I.D., 3 μ m) at 35 °C, and the eluent was aqueous formic acid (100:0.1, V/V) (A)-acetonitrile (B) at a flow rate of 0.3 mL/min. The gradient elution was performed as follows: 16%–33% B at 0–8 min, and 33%–99% B at 8–19 min. The capillary voltage was 3500 V/–4000 V. MS detection of the samples was performed by multiple reaction monitoring in both ion modes by comparison with reference standards. Drying gas temperature was set at 350 °C with a velocity of 9 L/min and nebuliser pressure at 40 psi. A MassHunter Workstation (Version B.06.00, Agilent Technologies) was used to process the data.

2.9.2. Nissl staining

After the behavioural study, three rats were randomly selected from each group. The rats were anaesthetised, and brain tissue from each rat was isolated on ice. The brain tissue was divided equally into two parts. One part was fixed in 4% paraformaldehyde solution for 24 h and then embedded in paraffin, and the other part was subjected to Golgi staining. The paraffin-embedded brain tissue was sliced into 5- μ m sections by serial sectioning using a microtome. The sections were dewaxed in xylene for 10 min and then treated sequentially with 100% ethanol, 90% ethanol, 70% ethanol and distilled water for 2 min each. Subsequently, the sections were stained with Nissl solution for 10 min, rinsed with distilled water for 2 min, dehydrated with gradient ethanol (70%–95%) for 2 min, and mounted using neutral gum. Sections were examined under a microscope and imaged. The number of neurons in the hippocampus was calculated for each group of rats using Image J software (Version 1.53).

2.9.3. Thioflavin-S staining

Thioflavin-S staining was used to examine A β deposition in the hippocampal region of rats in each group. Staining was performed in accordance with the method described in previous reports [37]. Briefly, paraffin-embedded brain tissue was sliced into 5- μ m sections using a microtome. The sections were deparaffinized using xylene and gradient ethanol (100%–75%), and washed with distilled water for 5 min. Sections were then incubated in thioflavin S solution for 10 min at room temperature, washed with PBS for 5 min, and subjected to nuclear counterstaining with 4',6-diamidino-2-phenylindole (DAPI). After being washed with PBS, the sections were mounted using an anti-fluorescence quenching mounting medium. The sections were examined and imaged using a fluorescence microscope. The number and average area of A β plaques and the proportion of thioflavin S-positive areas were analysed using Image J software. The proportion of thioflavin S-positive area was calculated using the following formula:

$$(\text{area of A}\beta \text{ plaques}/\text{total area of the selected region}) \times 100\%$$

2.9.4. ELISA

The hippocampus was homogenised in PBS (1:8, *m/V*) using a tissue homogeniser, and centrifuged at 4 °C and 12,000 rpm for 15 min. The supernatant was collected and the protein concentration of each sample was determined using a BCA protein assay kit. The expression levels of AMP, ATP, A β ₄₀ and A β ₄₂ in the hippocampus of various groups of rats were determined using ELISA kits in accordance with the manufacturers' instructions.

2.9.5. Golgi-Cox staining

Golgi-Cox staining was performed in accordance with the instructions of the FD Rapid GolgiStain Kit, as described previously [38]. Briefly, brain tissue was incubated in a mixture of solutions A and B for 14 days at room temperature in the dark. After being washed with distilled water, the brain tissue was transferred to solution C and incubated for 48 h at 4 °C in the dark. During the incubation period, the solution was changed every 24 h. Subsequently, the brain tissue was washed with distilled water for 5 min and stored at –80 °C until further processing. Sections (100 μ m-thick) were prepared using a cryostat microtome and dried overnight in the dark. The sections were sequentially treated with concentrated ammonia water and an acidic hard-film fixer for 15 min, washed with distilled water for 3 min, and sealed with

glycerin gelatin. The sections were examined and imaged using a confocal laser scanning microscope. The dendritic spine density and length of the neurons in the hippocampal CA3 region of the rats were measured using the Image J software. In addition, the complexity of neuronal dendrites in the hippocampal CA3 region was analysed using the Sholl Analysis plugin of Image J software [39,40].

2.9.6. Transmission electron microscopy (TEM)

The hippocampal tissue was collected and trimmed into tissue blocks (approximately 1 mm \times 1 mm \times 1 mm). The trimmed hippocampal tissue was fixed in 2.5% glutaraldehyde solution. Subsequently, the brain tissue was fixed in 1% osmium tetroxide for 2 h at room temperature in the dark, and the hippocampus was dehydrated using increasing gradients of ethanol (30%–100%). After being washed with PBS, the hippocampal tissues were embedded in Epon-812, cut into 70-nm sections using an ultramicrotome, and stained with 3% uranyl acetate and lead citrate. The treated cells were collected and centrifuged. The supernatants were discarded, and cells were fixed with 2.5% glutaraldehyde solution for 6 h. After centrifugation and removal of the supernatant, the cells were embedded in 1% agarose solution. The cells were then rinsed three times with PBS for 15 min each and fixed in 1% osmic acid for 2 h at room temperature in the dark. Subsequently, the cells were dehydrated using an ethanol gradient (30%–100%) and 100% acetone, following which they were embedded, sectioned, and stained. The ultrastructure of the mitochondria and synapses was examined using TEM. The morphology of mitochondria and the thickness and length of the postsynaptic density were analysed using Image J software [41,42].

2.9.7. Immunofluorescence staining

Paraffin-embedded brain tissue was cut into 5- μ m sections by serial sectioning using a microtome. The sections were deparaffinized in xylene and gradient ethanol (100%–75%) and then subjected to antigen retrieval for 30 min in ethylenediaminetetraacetic acid (EDTA) solution. The sections were washed with PBS, blocked with 3% bovine serum albumin (BSA), and incubated overnight with primary antibodies against PSD95 (1:100) and SYN1 (1:100) at 4 °C. Subsequently, the sections were washed with PBS and incubated with Cy3-labelled goat anti-rabbit secondary antibody (1:500) for 1 h at room temperature in the dark. The sections were washed again with PBS, counterstained with DAPI, and mounted using an anti-fluorescence quenching mounting medium. For cell immunofluorescence staining, the treated cells were collected, centrifuged at 3,500 rpm for 5 min, fixed with 4% paraformaldehyde for 15 min, centrifuged again, washed with PBS for 3 min, and permeabilised with 0.1% Triton-X100 for 20 min at room temperature. After permeabilization, the cells were blocked with 3% BSA at room temperature for 30 min and then incubated with diluted primary antibody at 4 °C overnight. Subsequently, the cells were incubated with a FITC-labelled goat anti-rabbit secondary antibody (1:500) for 50 min at room temperature in the dark. After counterstaining with DAPI, the cells were mounted using an anti-fluorescence quenching mounting medium. The slides were examined and imaged under a fluorescence microscope, and the average fluorescence intensities of PSD95 and SYN1 were calculated using the Image J software.

2.9.8. Tandem mass tag (TMT) label-based proteomics analysis of hippocampal tissue

Four rats from each group were randomly selected. Rat hippocampal tissue was isolated on ice and stored at –80 °C. The hippocampal tissue was homogenised in an appropriate amount of

protein lysis buffer (8 mol/L urea, 100 mmol/L Tris, 1 × protease inhibitor, pH 8.5) using a tissue grinder. After homogenisation, the tissues were centrifuged at 15,000 g and 4 °C for 10 min. The resulting supernatants were collected. Protein concentrations in the supernatants were determined using Bradford assay. The samples were digested with trypsin and desalted using reverse-phase column chromatography (HLB). After desalination, the samples were lyophilised, dissolved in triethylammonium bicarbonate (TEAB), and incubated at room temperature for 10 min. Subsequently, 100 µL of protein sample was added to each TMT bottle and incubated at room temperature for 1 h. Eight microlitres of 5% hydroxylamine was then added, followed by incubation at room temperature for 15 min. After labelling, the protein samples were immediately vacuum lyophilised and stored at –80 °C for future use.

The labelled samples were dissolved in 100 µL of acetonitrile and centrifuged at 14,000 g for 20 min. Supernatants were collected and subjected to reverse-phase chromatography gradient separation (Nano HPLC, Thermo Scientific EASY-nLC 1000 System) under high pH conditions. The isolated components were reconstituted using 20 µL of solution with 2% acetonitrile and 0.1% formic acid, and were centrifuged at 12,000 g for 10 min. Ten microlitres of the resulting supernatant were used for LC-MS/MS analysis. The mass spectrometry (Q-Exactive; Thermo Scientific) conditions were as follows: spray voltage, 2.41 kV; capillary temperature, 25 °C; ion source, EASY-Spray; a first-level full scan with a range of 350–1,600 *m/z*, a resolution of 70,000 FWHM and a scan time of 60 ms; and a secondary scan with a range of 350–1,600 *m/z*, a resolution of 17,500 FWHM, and a scan time of 70 ms. The mass spectrometry raw files were processed using Proteome Discoverer software (Version 1.4), and the collected data were interpreted using the UniProt Rat database (<https://www.uniprot.org/>). After filtering the raw data for the groups, a *t*-test was performed to identify differentially expressed proteins. Differentially expressed proteins were subjected to biological process (BP) enrichment analysis, cellular component (CC) enrichment analysis, molecular function (MF) enrichment analysis, and Kyoto Encyclopaedia of Genes and Genomes (KEGG) enrichment analysis using the DAVID database (Version 6.8, <https://david.ncifcrf.gov/>). Protein-protein interaction networks were analysed using the STRING database (Version 10.5, <https://cn.string-db.org/>).

2.9.9. Determination of ATP content in cells

The cellular ATP content was determined using an ATP detection kit. The treated cells were collected and centrifuged, and the supernatant was discarded. After addition of 500 µL of extraction buffer, the cells were sonicated for 1 min and centrifuged at 4 °C and 10,000 g for 10 min. The resulting supernatant was mixed with 500 µL of chloroform and centrifuged at 4 °C and 10,000 g for 5 min. The supernatant was collected and the cellular ATP content was determined in accordance with the instructions provided with the kit.

2.9.10. Examination of MMP and ROS in cells

Changes in MMP were evaluated using a MMP Assay Kit with JC-1, as previously described [43]. Briefly, the treated cells were collected and centrifuged. After removal of the supernatant, the cells were overlaid with 500 µL of JC-1 staining solution and incubated at 37 °C for 20 min. The cells were centrifuged again, and the supernatant was discarded. The cells were then washed three times with PBS for 3 min each and mixed with 500 µL of JC-1 staining buffer. The fluorescence intensity was analysed using a flow cytometer. The MMP levels were evaluated by calculating the ratio of red to green fluorescence (590/520). The ROS levels in each group of cells were measured using a ROS assay kit. Briefly, the

treated cells were collected and centrifuged. After removing the supernatant, cells were overlaid with 10 µM of 2,7-dichlorofluorescein-diacetate (DCFH-DA) and incubated at 37 °C for 20 min. After washing with PBS, the cells were collected by centrifugation. The fluorescence intensity of ROS was analysed using flow cytometry.

2.9.11. Labelling of mitochondria with MitoTracker red CMXRos

The mitochondria were labelled with MitoTracker Red CMXRos. The treated cells were collected and centrifuged. The resulting supernatant was discarded. The cells were then washed with PBS, mixed with 1 mL of MitoTracker Red CMXRos, and incubated for 30 min at 37 °C in the dark. Mitochondrial morphology was examined and imaged using a laser scanning confocal microscope. Mitochondrial length was analysed using Image J software [44].

2.9.12. Neuro-electrophysiological recording of cells

Standard techniques of electrophysiological studies were used in a manner that have been described in our previous studies [45]. SD rats were decapitated and their brains were quickly removed, glued to the chilled stage of a Vibroslice, and placed into ice-saline which was saturated with oxygen and sliced to a thickness of 350 µm. Slices were incubated in aCSF, which was saturated with 95% oxygen and 5% carbon dioxide at room temperature (24 °C). The slices were allowed to recover for at least 1 h before being transferred to the recording chamber. The standard aCSF solution contained (in mM): 140 NaCl, 10 glucose, and 10 HEPES, 5.0 KCl, 2.0 CaCl₂, 1.0 MgCl₂ (Flow rate = 2–3 mL/min). The pH of the solution was adjusted to 7.4. Most experiments were performed with whole-cell recording using a pipette solution that contained (in mM) 140 KCl, 10 HEPES, 4.0 EGTA, 2.0 Mg-ATP, 0.40 CaCl₂, 1.0 MgCl₂.

Synaptic currents were recorded using an Axopatch 200 B amplifier, which was interfaced via a Digidata 1320A (Axon Instruments) A/D converter. The recording was performed in voltage-clamp mode and directly digitised using pCLAMP 10 software for offline analysis. The pipette was pulled from glass pipettes, which was pulled to a tip of 1–2 µm using a vertical puller (Micro Forge MF830; Narishige). The pipette had a resistance of 3–5 MΩ. Routinely, 80% of the series resistance was compensated; hence, there was a 2–4 mV error for 1 nA of current. For long-term potential (LTP), a bipolar wire electrode was used to activate Schaffer collateral fibre, which was placed in the stratum radiatum on the hippocampal CA1 region, and the resulting field EPSPs (fEPSPs) on CA1 pyramidal cells were recorded using an extracellular glass microelectrode (filled with aCSF), which had a resistance 5–10 MΩ. Fast stimulation involved four bursts of five pulses at 100 Hz with interburst intervals.

2.9.13. Western blotting

Appropriate amounts of hippocampal tissue and cells were homogenised in RIPA lysis buffer using a tissue grinder. The homogenate was centrifuged at 4 °C and 12,000 rpm for 15 min, and the resulting supernatant was collected. The protein concentrations of the various samples were determined using a BCA protein assay kit. The protein solutions were mixed with 5 × reduced protein loading buffer at a ratio of 4:1, denatured in boiling water for 15 min, and stored at –20 °C until analysis. An 8% separating gel and 5% stacking gel were prepared following the instructions of the SDS-PAGE gel kit. Samples (30 µg each) were electrophoresed, and the proteins were transferred to a PVDF membrane. The membrane was blocked with 5% skimmed milk for 2 h and then incubated with primary antibodies (diluted with TBST according to the manufacturers' instructions) at 4 °C overnight. The antibodies used in this study are listed in Table 1. Subsequently, the membrane was washed three times (5 min each) with TBST and incubated with

Table 1
Details of antibodies used in Western blotting and immunofluorescence.

Antibodies	Catalog number	Host	Dilution	Provider
A β (B4)	sc-28365	Mouse	1:1000 for WB	Santa Cruz
ADAM10	ab1997	Rabbit	1:500 for WB	Abcam
BACE1	sc-33711	Mouse	1:1000 for WB	Santa Cruz
PS1	#5643	Rabbit	1:1000 for WB	Cell Signaling Technology
IDE	ab32216	Rabbit	1:1000 for WB	Abcam
PSD95	A6194	Rabbit	1:500 for WB 1:100 for IF	ABclonal Biotechnology
SYN1	#5297	Rabbit	1:1000 for WB 1:100 for IF	Cell Signaling Technology
PINK1	A11435	Rabbit	1:1000 for WB	ABclonal Biotechnology
Parin	A0968	Rabbit	1:1000 for WB	ABclonal Biotechnology
MFN1	A9880	Rabbit	1:1000 for WB	ABclonal Biotechnology
MFN2	A12771	Rabbit	1:1000 for WB	ABclonal Biotechnology
OPA1	A9833	Rabbit	1:1000 for WB	ABclonal Biotechnology
Drp1	A2586	Rabbit	1:1000 for WB	ABclonal Biotechnology
p-Drp1-Ser616	#3455	Rabbit	1:1000 for WB	Cell Signaling Technology
MFF	A4874	Rabbit	1:1000 for WB	ABclonal Biotechnology
β -actin	AC038	Rabbit	1:10,000 for WB	ABclonal Biotechnology

horseradish peroxidase (HRP)-conjugated goat anti-rabbit IgG (1:5000 dilution) at room temperature for 30 min. The membranes were washed three times (5 min each) with TBST. After washing, an enhanced chemiluminescence (ECL) reagent was added dropwise to the surface of the membrane. Protein bands were visualised and imaged using a gel imaging and analysis system. Band intensities of protein samples were quantified using Image J software and normalised using β -actin.

2.9.14. Molecular docking simulation experiments

Molecular docking, which has been widely used for drug discovery and designing, was used to verify the affinity of the interactions between the active ingredients of DZSM and relevant protein targets of mitochondrial dysfunction in AD. The three-dimensional (3D) structures of the proteins were obtained from the RCSB Protein Data Bank (PDB) and AlphFold databases. The sdf file format of the active ingredients obtained from PubChem (<https://pubchem.ncbi.nlm.nih.gov/>) was prepared and optimised using Chem3D for energy minimisation and structure optimisation. Docking was performed using Molecular Operating Environment (MOE) software (version 2019.01). The binding energies of the interactions were analysed and calculated using computer simulations. Docking models with binding affinities lower than -7.0 kcal/mol were selected, and a compound-target network was constructed using Cytoscape (Version 3.8.2). The “degree” calculated by linked edges can reflect the significance of nodes. The degree of each node and compound was analysed using the CytoHubba plugin in Cytoscape.

2.10. Statistical analysis

Experimental data were processed using the SPSS (Version 23.0) and GraphPad Prism (Version 9.0) softwares. All experimental results were expressed as mean \pm standard error of mean (mean \pm SEM). The experimental data were subjected to normality analysis using Shapiro-Wilk test. Data that did not conform to a normal distribution were analysed using Kruskal-Wallis test, and a P value < 0.05 indicated that the difference was statistically significant. Normally distributed data were analysed using one-way analysis of variance (ANOVA). For homogeneous variance (Levene > 0.05), between-group comparisons were performed using the LSD method. For nonhomogeneous variance (Levene < 0.05), between-group comparisons were performed using Tamhane's T2 method. A P value < 0.05 indicated that the difference was statistically significant.

3. Results

3.1. DZSM improved cognitive impairment in A β_{42} -induced AD rats

In the MWM test, the learning and memory skills of the rats were evaluated using place navigation and spatial probe tests, respectively (Fig. 1B). From the 1st to the 3rd day of the training period, no obvious changes were observed in terms of escape latency between the control group and the other three groups, and the difference was not statistically significant. From day 4, escape latency significantly increased in the AD group compared to the control group, and this phenomenon was reversed by DZSM (Fig. 1C). Fig. 1D shows the results of escape latency to reach the hidden platform on day five of the MWM test. The swimming tracks of the mice during the MWM test are shown in Fig. 1E. The spatial probe test results indicated that the times of crossing the platform and the time within the target quadrant were significantly reduced in the AD group in comparison to the control group. The aforementioned two parameters were increased in the AD + DZSM group in comparison to the AD group (Figs. 1F and G). In addition, the average swimming speed did not vary significantly among the various groups (Fig. 1H). Object placement in trials of the NOR task is presented in Fig. 1I. The time that the rats spent exploring objects A and B did not differ significantly among the groups (Figs. 1J and K). The NOI in the NOR test was significantly reduced in the AD group than in the control group. In contrast, the NOI increased after four weeks of DZSM treatment (Fig. 1L). These results indicate that an AD model was successfully established by administering injections of A β_{42} in the lateral ventricle and that DZSM improved the cognitive impairment induced by A β_{42} .

3.2. Screening the components of DZSM absorbed in rats

The prototype components of DZSM absorbed in rats could provide a chemical basis for investigation of the effective components. As shown in Figs. 2A–H, a total of 19 components were found in DZSM. Of these 19 components, ginsenoside Rd, ginsenoside F1, schizandrin, deoxyschizandrin, schisanhenol, and methyl-ophiopogonanone A, B were detected in rat plasma and CSF (except scutellarein which only appeared in plasma) after giving DZSM by comparing the chromatograms of UPLC-MS/MS between dosed and blank group. Detailed information on the characterised components of DZSM in the rat plasma and CSF is presented in Table 2.

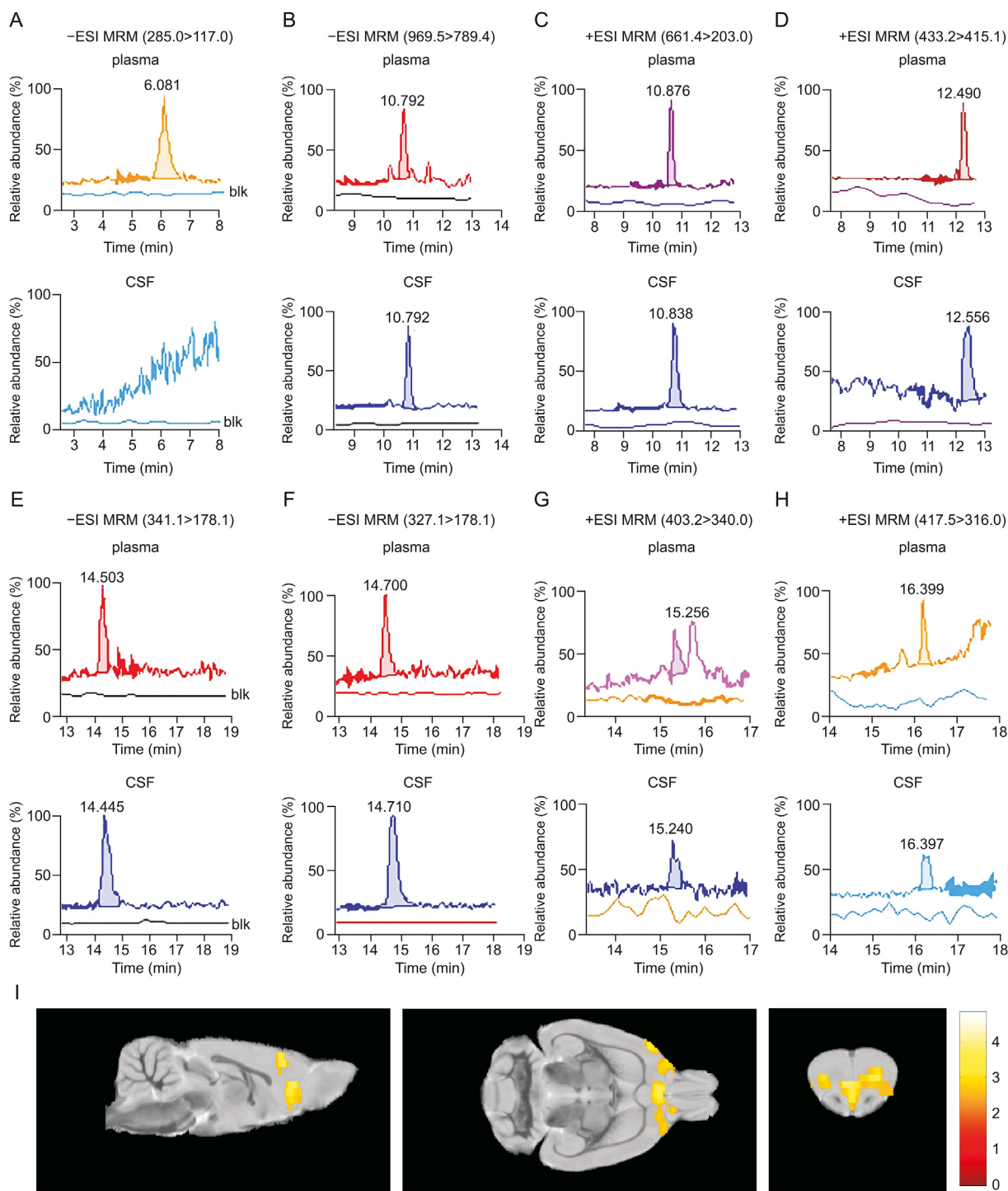


Fig. 2. Components in rats plasma and cerebrospinal fluid (CSF) were detected by ultra-performance liquid chromatography tandem mass spectrometry (UPLC-MS/MS) after Dengzhan Shengmai (DZSM) treatment. (A) scutellarein, (B) ginsenoside Rd, (C) ginsenoside F1, (D) schizandrin, (E) deoxyschizandrin, (F) schisanhenol, (G) methylophiopogonane A, (H) methylophiopogonane B. (I) Brain regions showing significant differences in fractional anisotropy (FA) between DZSM group and Alzheimer's disease (AD) group.

3.3. DZSM treatment protected cerebral white matter in specific regions in AD rats

To explore the changes in white matter integrity of AD rats after DZSM, voxel-based analyses were conducted on the

diffusion tensor metrics of FA and MD. The results showed that rats in the DZSM groups presented significant FA compared to AD rats. FA were clustered in the brain regions, including the primary cingular cortex, prelimbic system, primary visual cortex monocular area, dorsolateral orbital cortex, dysgranular insular

Table 2

The components detected from Dengzhan Shengmai (DZSM) and plasma/cerebrospinal fluid (CSF) in rats by ultra-performance liquid chromatography tandem mass spectrometry (UPLC-MS/MS).

No.	Compound	Transition	t_R	Plasma	CSF
1	Apigenin	431.10 → 268.00	4.637	–	–
2	Apigenin-7-O-glucuronide	445.07 → 268.90	4.692	–	–
3	Homoplantagin	461.11 → 282.90	4.974	–	–
4	Scutellarein	285.04 → 117.00	6.063	+	–
5	Ginsenoside Rg1	603.40 → 423.10	6.203	–	–
6	Ginsenoside Rf	823.48 → 365.00	9.251	–	–
7	Ginsenoside Rb1	1131.49 → 364.60	9.959	–	–
8	Ginsenoside Ro	979.49 → 641.30	10.290	–	–
9	Ginsenoside Re	969.54 → 789.40	10.778	–	–
10	Ginsenoside Rd	969.49 → 789.40	10.779	+	+
11	Ginsenoside F1	661.43 → 203.00	10.958	+	+
12	Schisandrin	433.22 → 415.10	12.505	+	+
13	Liriope muscari baily saponins C	915.60 → 737.50	12.768	–	–
14	Liriopeptides B	723.50 → 251.20	13.603	–	–
15	Methylphopogonone A	341.10 → 178.10	14.428	+	+
16	Methylphopogonone B	327.10 → 178.10	14.665	+	+
17	Schisanhenol	403.21 → 340.00	15.259	+	+
18	Deoxyschizandrin	417.52 → 316.00	16.402	+	+
19	Schisandrin C	385.17 → 285.00	17.190	–	–

–: undetected or under limit of quantification.

+: detected.

cortex, and cornu ammonis 3 (Fig. 2I). However, no significant differences were observed between the DZSM and AD groups in terms of MD. The different brain regions are shown in Table 3.

3.4. DZSM alleviated $A\beta_{42}$ -induced synaptic damage in the rat hippocampus

Golgi-Cox staining was performed to evaluate whether DZSM alleviated $A\beta_{42}$ -induced synaptic damage. Golgi staining revealed that the density and length of dendritic spines in the hippocampal CA3 region were significantly reduced in the AD group than in the control group. In contrast, the density and length of dendritic spines in the hippocampal CA3 region were significantly increased in the AD + DZSM group (Figs. 3A and B). The complexity of neuronal dendrites was analysed using the Sholl Analysis plugin in Image J software. Compared with the control group, the AD group had a significantly reduced number of dendritic branches in the hippocampal CA3 region, which were 150–250 μm from the neuron body. This phenomenon was reversed after four weeks of DZSM treatment (Figs. 3C and D).

Subsequently, we examined the expression of synaptic marker proteins, PSD95 and SYN1, in the hippocampus using immunofluorescence (Figs. 3E and F) and Western blotting (Figs. 3G and H). Compared with those in the control group, the expression levels of PSD95 and SYN1 in the hippocampus of rats in the AD group were significantly decreased. Compared with the AD group, the AD + DZSM group showed increased expression levels of PSD95 and SYN1 in the hippocampus. The above results indicated that

DZSM alleviated $A\beta_{42}$ -induced hippocampal synaptic damage. In addition, we examined the ultrastructure of synapses in the hippocampal CA3 region using TEM and calculated the length and width of postsynaptic density using Image J software. As shown in Figs. 3I and J, the length and width of the postsynaptic density in the hippocampal CA3 region were significantly reduced in the AD group compared to the control group. Compared to the AD group, the length and width of the postsynaptic density in the hippocampal CA3 region were increased in the AD + DZSM group. Together, these data illustrated that DZSM had an inhibitory effect on $A\beta_{42}$ -induced hippocampal synaptic damage.

3.5. DZSM inhibited hippocampal neuronal loss and $A\beta$ deposition by regulating $A\beta$ -related degradative enzymes in AD rats

MRI and UPLC-MS/MS revealed that DZSM ameliorated $A\beta_{42}$ -induced hippocampal structural damage and that the active components of DZSM penetrated the blood-brain barrier and entered the brain. To evaluate whether DZSM inhibited neuronal loss, Nissl staining was performed to label the neurons in the hippocampal region, and Image J software was used to count the number of neurons in the hippocampal CA1 and CA3 regions (Fig. 4A). The number of neurons in the hippocampal CA3 region of rats decreased after administration of the lateral ventricle injection of $A\beta_{42}$, and the number of neurons in the hippocampal CA3 region increased after four weeks of DZSM treatment. In contrast, no drastic changes were observed in the number of neurons in the hippocampal CA1 region among the various groups, and the

Table 3

Results of voxel-based analyses on fractional anisotropy (FA).

Brain regions	Cluster size	Coordinate			P
		X (mm)	Y (mm)	Z (mm)	
Primary cingular cortex ^b	110	0.5	3.7	4.4	<0.001
Prelimbic System ^a	343	–0.7	0.4	5.2	<0.001
Primary visual cortex monocular area ^a	146	–3.3	–6.2	6.8	<0.001
Dorsolateral orbital cortex	84	–3.3	5.3	2.8	<0.001
Dysgranular insular cortex	40	–5.4	3.7	2.0	<0.001
Cornu ammonis 3	55	–4.9	–2.9	3.6	<0.001

^a Multiple comparison corrected $P < 0.05$ (uncorrected $P < 0.01$, cluster size ≥ 146).

^b Margins significant after multiple comparison correction (corrected $P = 0.054$).

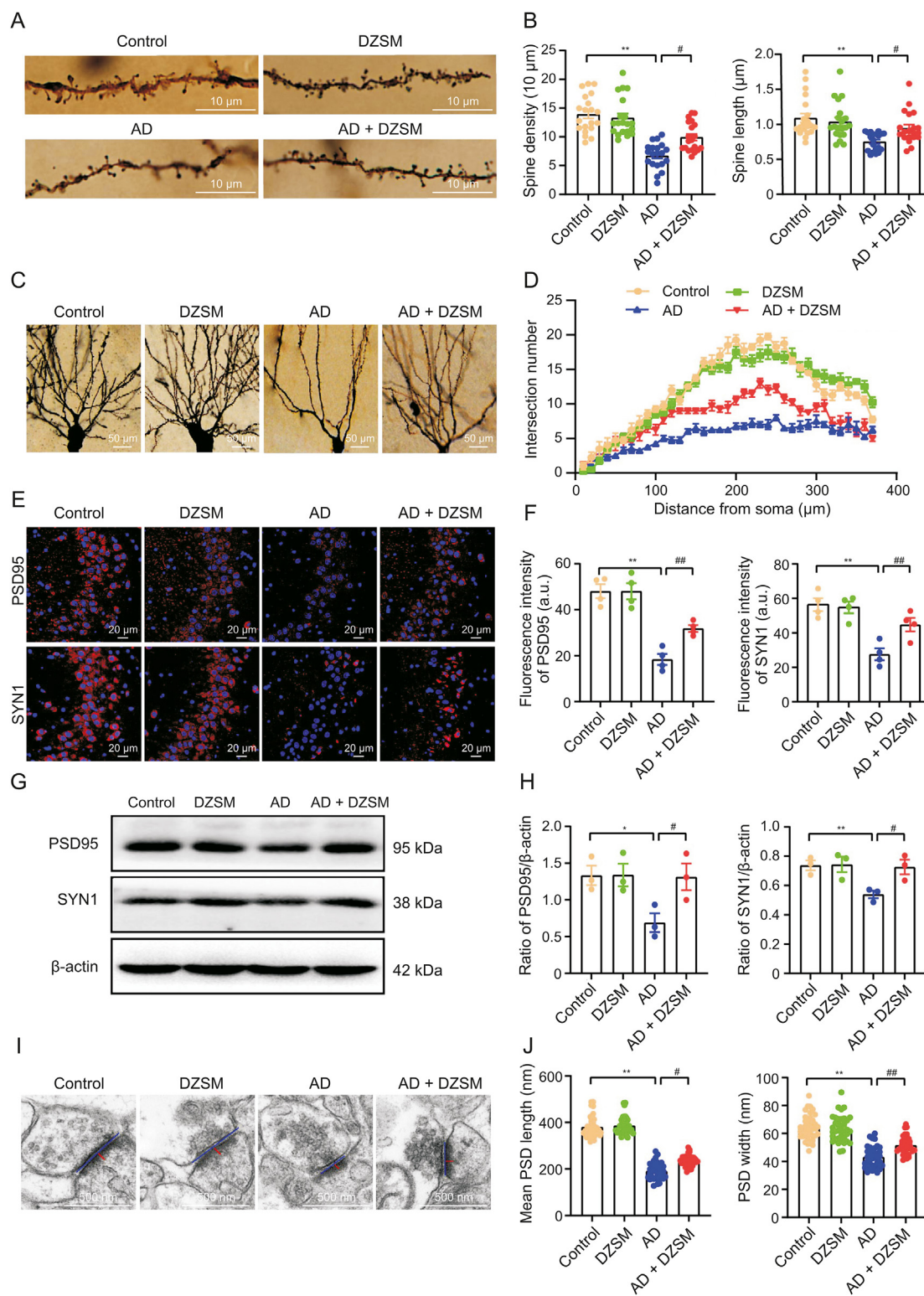


Fig. 3. Dengzhan Shengmai (DZSM) alleviates Aβ₄₂-induced hippocampal synaptic damage. (A) Representative Golgi staining of the hippocampal CA3 region (magnification = 1000 ×). (B) Quantitative analysis of the density and length of dendritic spines in hippocampal CA3 neurons (for each neuron, 5 dendrites were randomly selected and analysed, n = 4). (C) Representative Golgi staining of the hippocampal CA3 region (magnification = 200 ×). (D) Line chart for the dendritic complexity analysis of neurons in the hippocampal CA3 region (5 neurons were randomly selected from each slide and analysed, n = 4). (E) Representative immunofluorescence staining of PSD95 and SYN1 in the hippocampal CA3 region (magnification = 400 ×). (F) Quantitative analysis of the mean fluorescence intensity of PSD95 and SYN1 in the hippocampal CA3 region (n = 4). (G) Representative protein electrophoresis bands of PSD95 and SYN1 in the hippocampus. (H) Quantitative analysis of the protein expression levels of PSD95 and SYN1 in the hippocampus (n = 3). (I) Representative transmission electron microscope (TEM) images of the hippocampal CA3 region (magnification = 20,000 ×). The blue straight line indicates the length of the postsynaptic density (PSD), and the red straight line indicates the width of the PSD. 12 to 13 synapses were randomly selected from each slide for analysis. (J) Quantitative analysis of the length and width of the postsynaptic density in the hippocampal CA3 region (n = 3). The experimental data are expressed as the mean ± standard error of mean (SEM), n = 3 or 4. **P < 0.01 vs. Control group, and #P < 0.05 and ##P < 0.01 vs. AD group. AD: Alzheimer's disease.

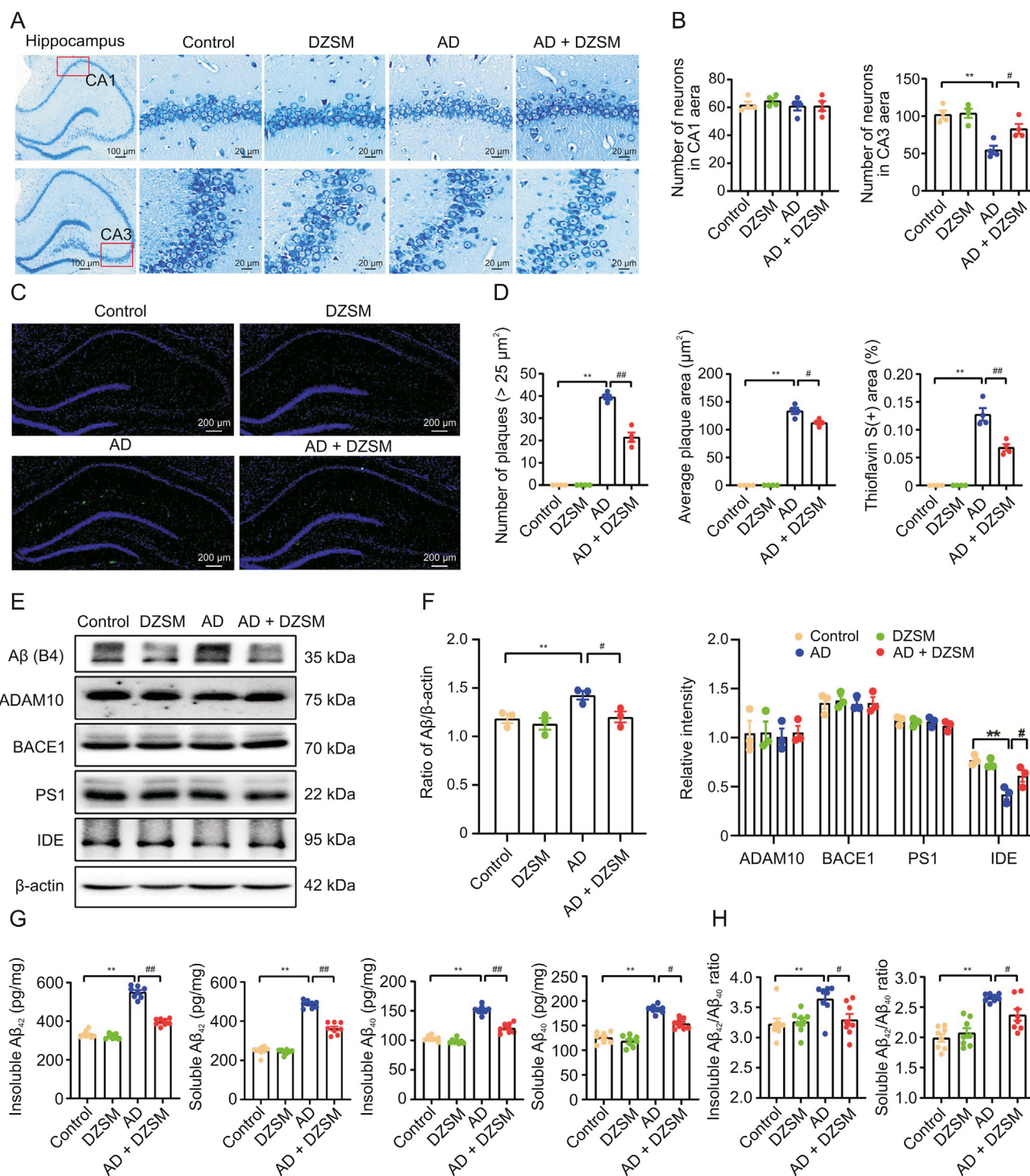


Fig. 4. Dengzhan Shengmai (DZSM) inhibits Aβ₄₂-induced hippocampal neuronal loss and Aβ deposition by regulating Aβ-related degradative enzymes. (A) Representative Nissl staining of the hippocampal CA1 and CA3 regions (magnification = 400 ×). (B) Quantitative analysis of the number of neurons in the hippocampal CA1 and CA3 regions (n = 4). (C) Representative thioflavin S staining of the hippocampus (magnification = 400 ×). (D) Statistical histograms showing the number and average area of Aβ plaques and the proportion of thioflavin S-positive area in the hippocampus (n = 4). (E) Representative protein electrophoresis bands of Aβ, Aβ-related secretases (ADAM10, BACE1, and PS1) and IDE in the hippocampus. (F) Quantitative analysis of the protein expression of Aβ, ADAM10, BACE1, PS1, and IDE in the hippocampus (n = 3). (G) The expression levels of insoluble/soluble Aβ₄₂ and insoluble/soluble Aβ₄₀ in the hippocampus (n = 8). (H) Statistical histogram showing the ratios of insoluble Aβ₄₂ to Aβ₄₀ and soluble Aβ₄₂ to Aβ₄₀ in the hippocampus (n = 8). Experimental data are expressed as the mean ± standard error of mean (SEM), n = 3, 4 or 8. **P < 0.01 vs. Control group, and #P < 0.05 and ###P < 0.01 vs. AD group. AD: Alzheimer's disease.

differences were not statistically significant (Fig. 4B). These data suggest that DZSM alleviated A β_{42} -induced hippocampal neuronal loss in AD rats. Image J software was used to calculate the number and average area of A β plaques and the proportion of thioflavin S-positive area in the hippocampal region (Fig. 4C). As shown in Fig. 4D, the number and average area of A β plaques and proportion of thioflavin S-positive area was significantly increased in the hippocampus of AD rats in comparison to those in the hippocampus of rats in the control group. These phenomena significantly improved after four weeks of DZSM treatment.

Western blotting was used to examine the expression of A β protein in the hippocampus of rats in each group. The results indicated that the expression of A β increased in the hippocampus of rats in the AD group. Compared with the AD group, rats in the DZSM group had a lower level of A β expression in the hippocampus (Figs. 4E and F). The deposition of A β is mainly related to A β_{40} and A β_{42} . Therefore, we used ELISA to examine the expression levels of insoluble/soluble A β_{40} and insoluble/soluble A β_{42} in the hippocampus of rats in each group and calculated the ratios of soluble A β_{42} /A β_{40} and insoluble A β_{42} /A β_{40} . As shown in Figs. 4G and H, compared with those in the hippocampus of rats in the control group, the expression levels of insoluble/soluble A β_{40} and insoluble/soluble A β_{42} in the hippocampus of rats in the AD group were found to be significantly increased. The ratios of soluble A β_{42} to A β_{40} and insoluble A β_{42} to A β_{40} were also significantly increased. In contrast, the above phenomena were reversed by DZSM treatment. A β production is regulated by A β -related secretases (such as ADAM10, BACE1 and PS1) and degradative enzymes (such as IDE). Therefore, we conducted Western blot analysis to examine the expression levels of ADAM10, BACE1, PS1, and IDE in the hippocampi of the rats in each group. The expression of IDE in the hippocampus of rats in

the AD group was lower than that in the hippocampus of rats in the control group but higher in the AD + DZSM group than in the AD group. In contrast, there were no drastic changes in the expression of ADAM10, BACE1, and PS1 in the hippocampus among the groups, and these differences were not statistically significant. These results indicate that DZSM improved A β_{42} -induced neuronal loss and that the underlying mechanism might be related to the regulation of A β -related degradative enzymes.

3.6. DZSM alleviated A β_{42} -induced synaptic activity in the rat hippocampus

To investigate synaptic transmission in the hippocampus, we performed whole-cell recordings of hippocampal slices. The results showed that A β_{42} significantly reduced the synaptic activities, as can be seen in the recordings of spontaneous synaptic currents (Fig. 5A). DZSM treatment significantly increased the frequency and amplitude of synaptic transmission (Figs. 5B and C). Then we tested the LTP in the hippocampus (Fig. 5D), and found that A β_{42} significantly reduced the memory ability, and the same stimulation-induced LTP was much smaller in A β_{42} treated rats. In contrast, DZSM reversed the effect, by increasing the amplitude of LTP from $135.5\% \pm 3.2\%$ to $167.3\% \pm 4.5\%$ (Figs. 5E and F).

3.7. The effect of DZSM on hippocampal proteomics

To explore the therapeutic effect of DZSM on AD, we used proteomics to analyse differentially expressed proteins in the hippocampus among the groups. Proteomic analysis of the hippocampus revealed 407 differentially expressed proteins between the AD and AD + DZSM groups (Table S1). First, we performed Gene Ontology

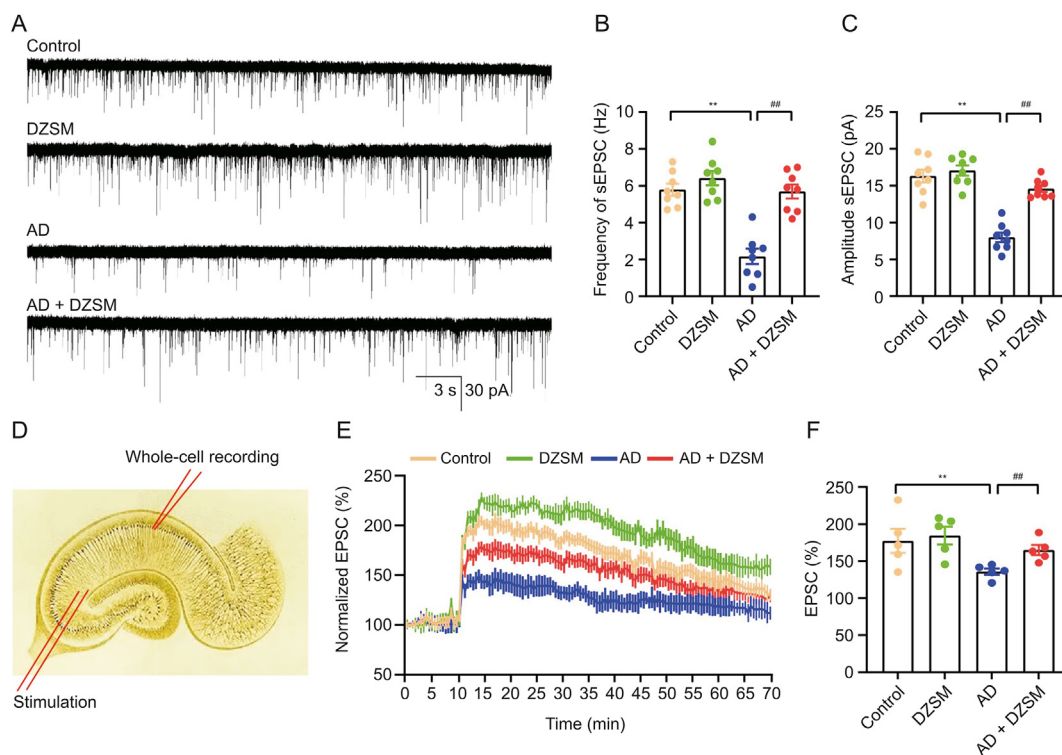


Fig. 5. Dengzhan Shengmai (DZSM) improves synaptic transmission and long-term potential in hippocampus. (A) Typical traces of spontaneous excitatory post-synaptic currents (sEPSC) in control, DZSM, Alzheimer's disease (AD) and AD + DZSM. (B,C) Statistical analysis of the frequency (B) and amplitude (C) of the synaptic currents ($n = 5$). (D) Schematic model shows the long-term potential (LTP) stimulation and recordings in hippocampus. (E) Statistical analysis of LTP in the four groups ($n = 5$). (F) Statistical comparison among the four groups for the LTP, and the highest amplitude was compared among the groups. ** $P < 0.01$ vs. Control group, and ** $P < 0.01$ vs. AD group.

(GO) term analysis of the differentially expressed proteins using the DAVID database, which allowed us to clarify the biological characteristics of the differentially expressed proteins. In this study, we analysed the biological characteristics of the top ten GO terms. The top 10 terms in the biological process analysis were: chemical synaptic transmission (17 proteins), platelet degranulation (13 proteins), regulation of macroautophagy (9 proteins), gluconeogenesis (9 proteins), mitochondrial respiratory chain complex I assembly (9 proteins), glycolytic process (8 proteins), substantia nigra development (8 proteins), neurotransmitter secretion (8 proteins), phagosome acidification (7 proteins), and ATP hydrolysis coupled proton transport (7 proteins) (Fig. 6A). The top 10 terms in the cellular component analysis were: extracellular exosome (135 proteins), cytosol (116 proteins), membrane (77 proteins), mitochondrion (57 proteins), myelin sheath (39 proteins), mitochondrial inner membrane (29 proteins), neuron projection (19 proteins), postsynaptic density (17 proteins), synaptic vesicle (15 proteins), and terminal bouton (11 proteins) (Fig. 6B).

The top five terms in the molecular function term analysis were: protein binding (182 proteins), poly(A) RNA binding (40 proteins), identical protein binding (28 proteins), calmodulin binding (18

proteins), and cadherin binding involved in cell-cell adhesion (17 proteins) (Fig. 6C). We performed KEGG analysis using the DAVID database. The results showed that the diseases regulated by DZSM were mainly neurodegenerative diseases, of which Huntington's disease (HD, 18 genes), AD (16 genes), and PD (15 genes) were the top three. KEGG analysis indicated that the therapeutic effect of DZSM on neurodegenerative diseases is mainly related to the metabolic pathways regulated by DZSM, namely, the metabolic pathways (46 genes), oxidative phosphorylation (18 genes), biosynthesis of enediyne antibiotics (18 genes), carbon metabolism (16 genes), glycolysis/gluconeogenesis (10 genes), biosynthesis of amino acids (8 genes), and the citrate cycle (TCA cycle) (6 genes). The main organismal systems of DZSM in the treatment of neurodegenerative diseases included the synaptic vesicle cycle (17 genes), collecting duct acid secretion (7 genes), and endocrine and other factor-regulated calcium reabsorption (6 genes) (Fig. 6D). GO term and KEGG analysis showed that DZSM was capable of improving neuronal damage and synaptic dysfunction in AD. This result was consistent with the aforementioned conclusions. Hippocampal proteomic analysis showed that DZSM acted on the mitochondrial membrane and regulated signalling pathways

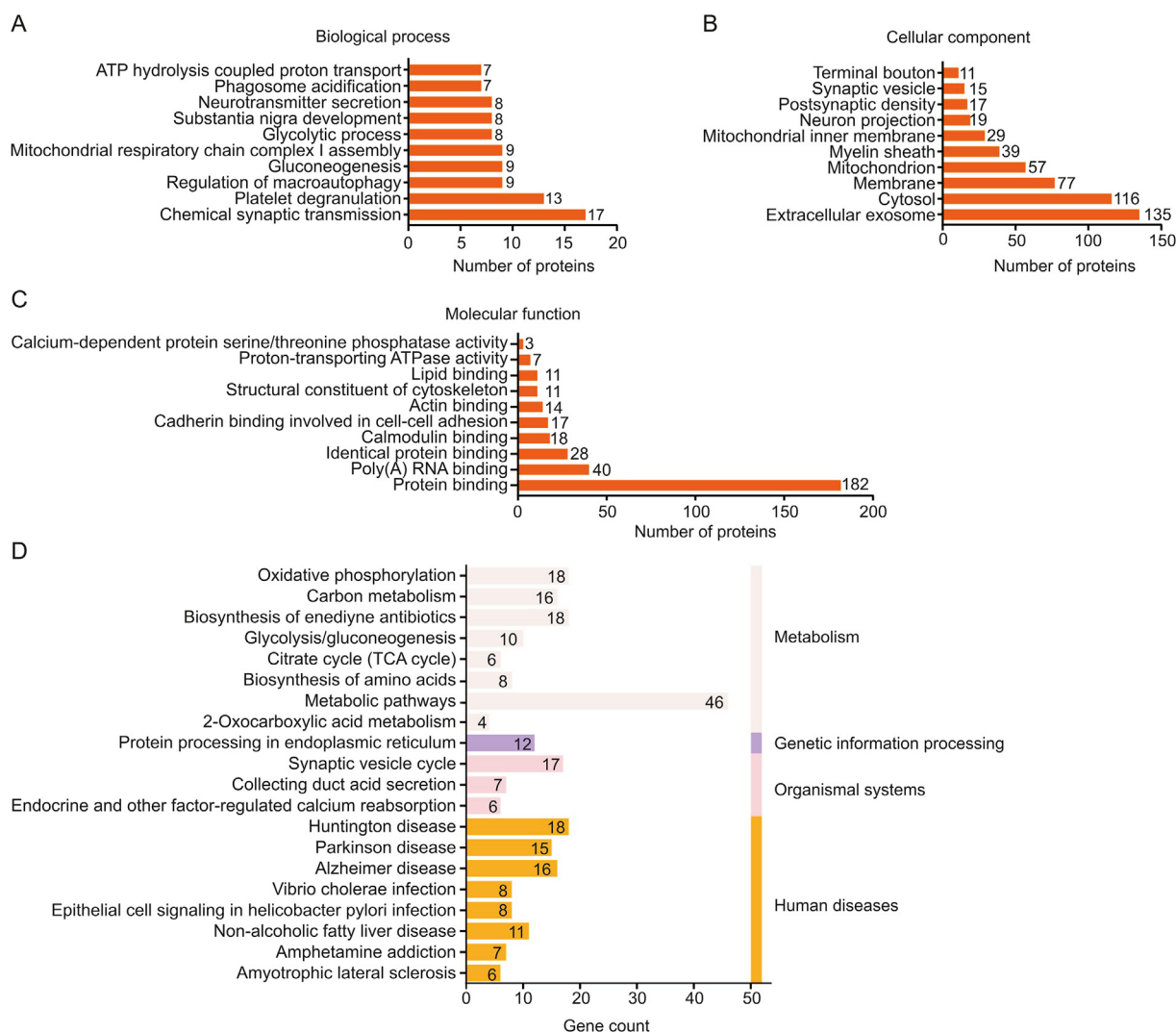


Fig. 6. The effect of Dengzhan Shengmai (DZSM) on hippocampal proteomics. (A) The results of the biological process (BP) analysis of differentially expressed proteins. (B) The results of the cellular component (CC) analysis of differentially expressed proteins. (C) The results of the molecular function (MF) analysis of differentially expressed proteins. (D) The results of the Kyoto Encyclopaedia of Genes and Genomes (KEGG) enrichment analysis of differentially expressed proteins.

related to energy metabolism. Therefore, we speculated that the therapeutic effect of DZSM on AD might be related to its ability to regulate mitochondrial function.

3.8. DZSM alleviates $A\beta_{42}$ -induced mitochondrial dysfunction by regulating mitophagy and mitochondrial fusion and fission

Hippocampal proteomic analysis showed that DZSM exerted its therapeutic effect on AD by regulating mitochondrial function. However, the mechanism of action of DZSM has not been completely elucidated. To explore the molecular mechanism of DZSM in AD, the ultrastructure of mitochondria was examined using TEM, and the length and area of the mitochondria were calculated using Image J software. As seen in Figs. 7A and B, the length and area of mitochondria in the hippocampal CA3 region were significantly reduced in the AD group in comparison to the control group, indicating that the lateral ventricle injection of $A\beta_{42}$ induced mitochondrial fragmentation. After four weeks of DZSM treatment, the length and area of the mitochondria increased in the hippocampal CA3 region. DZSM increased the AMP and ATP levels in the hippocampi of AD rats (Fig. 7C). The above results indicate that DZSM alleviated $A\beta_{42}$ -induced mitochondrial dysfunction and improved mitochondrial dysfunction and fragmentation.

As shown in Figs. 7D and E, the expression levels of PINK1 and Parkin in the hippocampus were significantly reduced in the AD group than in the control group. DZSM enhanced the expression of PINK1 and Parkin. These results indicate that $A\beta_{42}$ induced mitophagy defects in AD whereas DZSM activated mitophagy. The continuous fusion and fission of the mitochondria determines their morphology and distribution, and are prerequisites for mitochondrial function. Loss of the dynamic balance between mitochondrial fusion and fission leads to impaired mitochondrial function and fragmentation [20,46]. Previous studies have shown that the levels of mitochondrial fusion proteins, such as mitofusin 1 (MFN1), mitofusin 2 (MFN2), and optic atrophy protein 1 (OPA1), are decreased, whereas the levels of mitochondrial fission proteins, such as p-Drp1 and mitochondrial fission factor (MFF), are increased in AD [47–49]. Mitochondrial fragmentation was also reported to be increased. This evidence strongly suggests that a dynamic imbalance between mitochondrial fusion and fission is closely related to the pathological changes associated with AD. As seen in Figs. 7F–I, the expression levels of MFN1, MFN2 and OPA1 significantly decreased in the rat hippocampus after the lateral ventricle injection of $A\beta_{42}$, and the expression levels of MFF and phosphorylated p-Drp1 significantly increased. These results are consistent with TEM results, both of which collectively confirmed that $A\beta_{42}$ induced mitochondrial dysfunction and fragmentation. This phenomenon was reversed after four weeks of DZSM treatment. These results indicate that DZSM improved $A\beta_{42}$ -induced mitochondrial dysfunction and fragmentation by regulating mitochondrial fusion and fission. Based on the aforementioned results, we inferred that DZSM alleviated $A\beta_{42}$ -induced mitochondrial dysfunction by regulating mitophagy and mitochondrial fusion/fission.

3.9. DZSM alleviated $A\beta_{42}$ -induced synaptic dysfunction in primary neural cells

To further explore the molecular mechanisms by which DZSM improves synaptic plasticity in AD, $A\beta_{42}$ -injured primary neural cells were used as *in vitro* AD models. First, we treated the primary neural cells with various concentrations of $A\beta_{42}$ for 6, 12, 24 and 48 h. The results indicated that the incubation of primary neural

cells with either 5 μ M or 10 μ M $A\beta_{42}$ for 24 and 48 h significantly reduced cell viability (Fig. S1A). Subsequently, primary neural cells were treated with different concentrations of DZSM-containing serum for 6, 12, 24, and 48 h. The results showed that, compared to the control group, the viability of primary neural cells significantly increased after incubation with 10% DZSM-containing serum for 24 h (Fig. S1B). Finally, we treated $A\beta_{42}$ (5 μ M, 10 μ M)-injured primary neural cells with 10% DZSM-containing serum for 24 h. The results showed that 10% DZSM-containing serum significantly increased the viability of $A\beta_{42}$ (10 μ M, 24 h)-injured primary neural cells (Figs. S1C–F). Therefore, we selected 10 μ M $A\beta_{42}$ and 10% DZSM-containing serum as the experimental conditions, and the treatment time was 24 h. Previous studies have demonstrated that $A\beta_{42}$ (concentration ≥ 10 μ M, incubation time ≥ 24 h) induces primary neural cell apoptosis and necrosis, and reduces their synaptic plasticity. In this study, we examined the changes in synaptic plasticity in various groups of cells using neuroelectrophysiological approaches.

In addition, we examined the expression levels of PSD95 and SYN1 using immunofluorescence (Figs. 8A and B) and Western blotting (Figs. 8C and D). The expression levels of SYN1 and PSD95 were significantly decreased in the $A\beta_{42}$ group in comparison to the control group. Compared with those in the $A\beta_{42}$ group, the expression levels of SYN1 and PSD95 in the $A\beta_{42}$ + DZSM and $A\beta_{42}$ + Mdivi1 groups were increased. The above results demonstrated that DZSM alleviated $A\beta_{42}$ -induced synaptic dysfunction in primary neural cells.

3.10. DZSM alleviates $A\beta_{42}$ -induced mitochondrial dysfunction in primary neural cells

ROS expression levels were examined in each cell group. As seen in Fig. 9A, ROS expression was significantly increased in the $A\beta_{42}$ group in comparison to the control group. Cellular ROS expression was decreased in the $A\beta_{42}$ + DZSM and $A\beta_{42}$ + Mdivi1 groups compared to that in the $A\beta_{42}$ group. Reduced MMP and ATP content are also important manifestations of mitochondrial dysfunction. Therefore, we also examined the MMP in each group of cells using JC-1 and quantified the cellular ATP content using an ATP detection kit. As shown in Figs. 9B and C, the MMP and ATP contents were significantly decreased in the $A\beta_{42}$ group in comparison to the control group. The MMP and ATP contents in the cells increased after treatment with DZSM-containing serum. After accumulating in cells, ROS causes mitochondrial DNA damage and mutations, and also induces mitochondrial structural damage. We labelled the mitochondria using MitoTracker Red CMXRos and calculated their length using Image J software. The results showed that the length of mitochondria was decreased in the $A\beta_{42}$ group compared to that in the control group. In contrast, the length of mitochondria was increased in the $A\beta_{42}$ + DZSM and $A\beta_{42}$ + Mdivi1 groups (Fig. 9D). The above results demonstrated that $A\beta_{42}$ induced mitochondrial fragmentation, while DZSM improved $A\beta_{42}$ -induced mitochondrial fragmentation. In addition, we examined the ultrastructure of mitochondria in various groups of cells using TEM and calculated their length and area using Image J software. As shown in Fig. 9E, the length and area of mitochondria were significantly reduced in the $A\beta_{42}$ group in comparison to the control group. The length and area of mitochondria increased after treatment with DZSM-containing serum. This result was consistent with the above conclusions, indicating that DZSM improved $A\beta_{42}$ -induced mitochondrial fragmentation. In summary, DZSM alleviated $A\beta_{42}$ -induced mitochondrial dysfunction and fragmentation in primary neural cells.

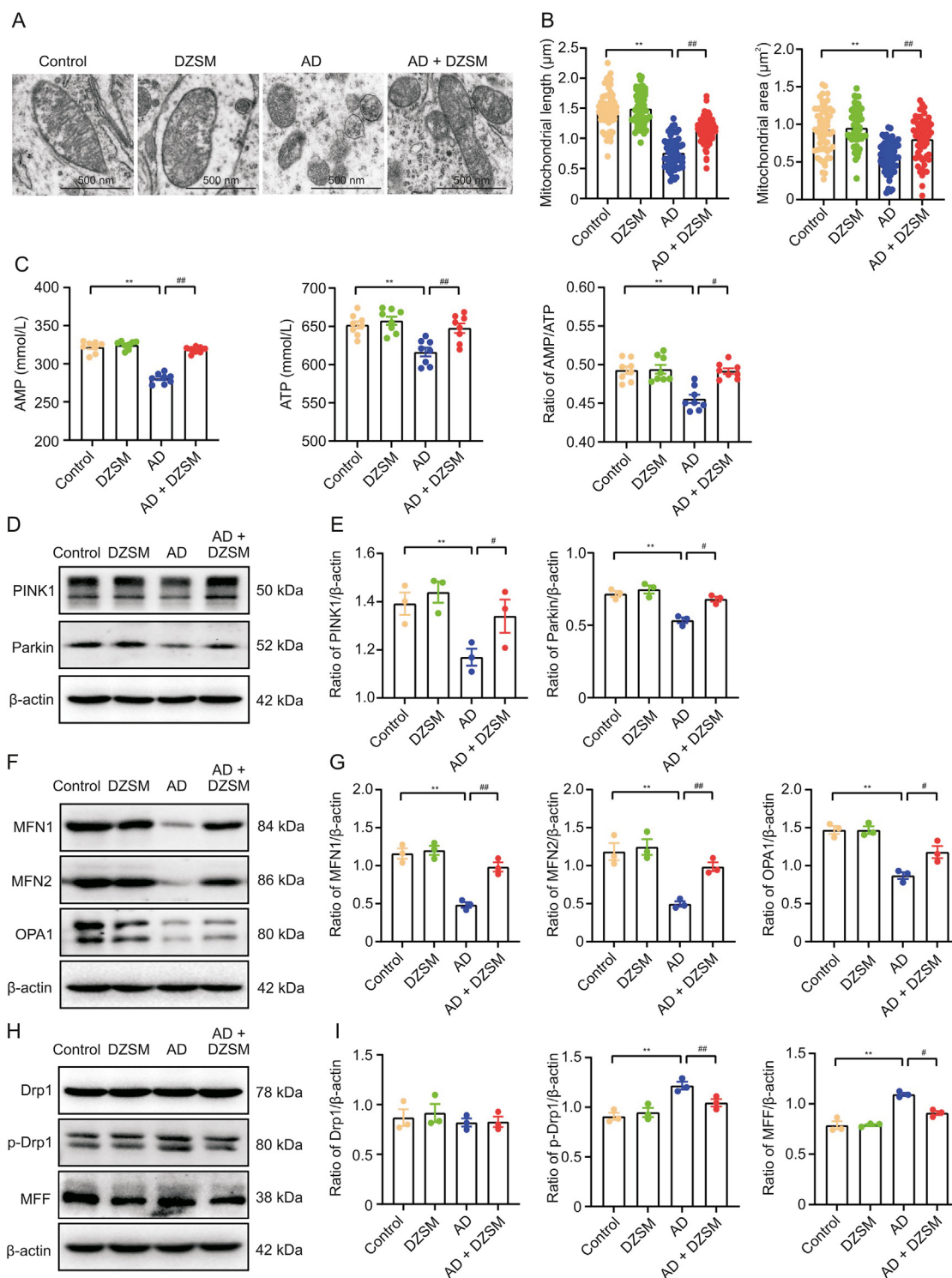


Fig. 7. Dengzhan Shengmai (DZSM) alleviates the A β_{42} -induced mitochondrial dysfunction by regulating mitophagy and mitochondrial fusion and fission. (A) Representative transmission electron microscopy (TEM) images of mitochondria in the hippocampal CA3 region (magnification = 7000 \times). (B) Quantitative analysis of the relative length and area of mitochondria in the hippocampal CA3 region ($n = 3$). (C) The expression levels of AMP and ATP and the AMP/ATP ratio in the hippocampus ($n = 8$). (D) Representative protein electrophoresis bands of PINK1 and Parkin in the hippocampus. (E) Quantitative analysis of the protein expression levels of PINK1 and Parkin in the hippocampus ($n = 3$). (F) Representative protein electrophoresis bands for MFN1, MFN2, and OPA1 in the hippocampus. (G) Quantitative analysis of the protein expression levels of MFN1, MFN2, and OPA1 in the hippocampus ($n = 3$). (H) Representative protein electrophoresis bands for Drp1, p-Drp1, and MFF in the hippocampus. (I) Quantitative analysis of the protein expression levels of p-Drp1/Drp1 and MFF in the hippocampus ($n = 3$). Experimental data are expressed as the mean \pm standard error of mean (SEM), $n = 3$ or 8. ** $P < 0.01$ vs. Control group, and # $P < 0.05$ or ## $P < 0.01$ vs. AD group. AD: Alzheimer's disease.

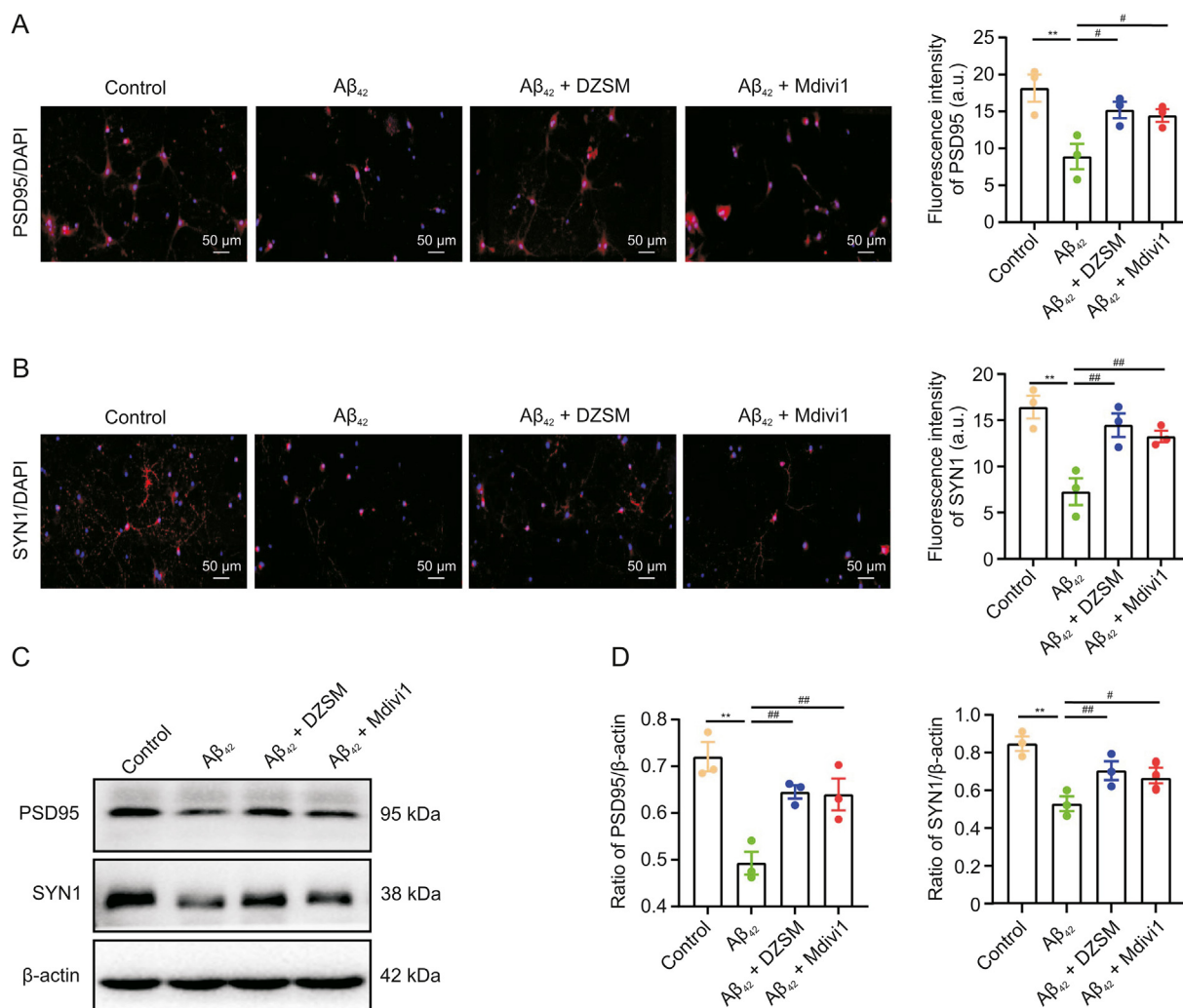


Fig. 8. Dengzhan Shengmai (DZSM) alleviates A β_{42} -induced synaptic dysfunction in primary neural cells. (A,B) Representative immunofluorescence images of PSD95 (A) and SYN1 (B) staining in cells (magnification = 400 \times), and quantitative analysis of the mean fluorescence intensity of PSD95 and SYN1 in cells ($n = 3$). (C) Representative protein electrophoresis bands for PSD95 and SYN1 in various groups of cells. (D) Quantitative analysis of the protein expression levels of PSD95 and SYN1 in cells ($n = 3$). Experimental data are expressed as the mean \pm standard error of mean (SEM), $n = 3$. ** $P < 0.01$ vs. Control group, and # $P < 0.05$ and ## $P < 0.01$ vs. A β_{42} group.

3.11. DZSM alleviates A β_{42} -induced mitochondrial dysfunction and fragmentation by regulating mitophagy and Drp1-mediated mitochondrial fission

In this study, we treated AD cells with a mitochondrial fission inhibitor (Mdivi1) *in vitro*. As seen in Figs. 10A and B, the expression levels of PINK1 and Parkin were significantly reduced in the A β_{42} group in comparison to the control group, and DZSM and Mdivi1 increased the expression levels of PINK1 and Parkin. These results indicated that DZSM activated mitophagy. In addition, we examined the expression levels of proteins related to mitochondrial fusion and fission by Western blotting. As seen in Figs. 10C and D, the expression levels of MFN1, MFN2, and OPA1 were significantly decreased in the A β_{42} group in comparison to the control group. In contrast, the expression levels of MFN1, MFN2 and OPA1 were higher in the A β_{42} + DZSM and A β_{42} + Mdivi1 groups than in the A β_{42} group. In addition, the expression levels of p-Drp1 and MFF decreased after treatment with DZSM-containing serum and Mdivi1 (Figs. 10E and F). The results demonstrated that DZSM alleviated A β_{42} -induced mitochondrial dysfunction and fragmentation by regulating mitophagy and Drp1-mediated mitochondrial fission.

3.12. Molecular docking results

The docking results are presented in a heat map (Fig. S2). A lower docking energy indicates stronger affinity between proteins and ligands. The drug-target binding affinity and best-scored docked position between ginsenoside Rd and (ADAM10, BACE1, IDE, Drp1); 4,5-O-dicaffeoylquinic acid and (SYN1, Drp1); schizandrin and (IDE, Parkin, Drp1); deoxyschizandrin and Drp are indicated in Figs. S3 and S4. The compound-target network is shown in Fig. S5A. The degree of compounds and protein targets is shown in Figs. S5B and C, respectively.

To some extent, these results support the reliability of WB, and reveal specific interactions between ingredients and protein targets. Accordingly, it was speculated that the active ingredients of DZSM exert biological effects by binding to specific sites on the relevant target proteins of mitochondrial dysfunction in AD.

4. Discussion

The current pharmaceutical interventions for AD often focus on symptom management rather than addressing the underlying pathology. This highlights the need for innovative strategies that

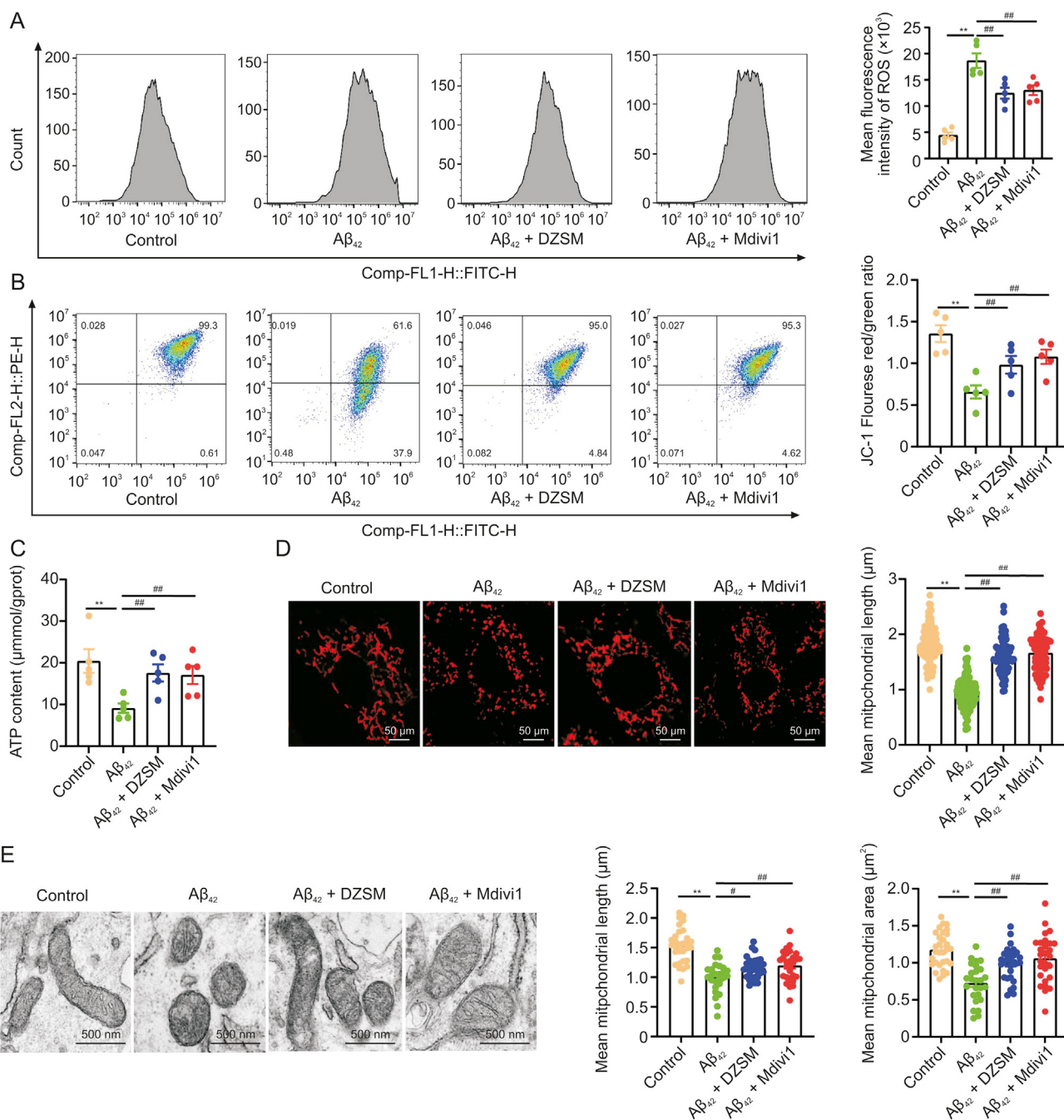


Fig. 9. Dengzhan Shengmai (DZSM) alleviates Aβ₄₂-induced mitochondrial dysfunction in primary neural cells. (A) Representative flow cytograms and quantitative analysis of cellular reactive oxygen species (ROS). (B) Representative flow cytograms of cellular mitochondrial membrane potential (MMP) and the quantitative analysis of the ratio of red to green fluorescence. (C) Statistical histogram of cellular ATP content. (D) Representative images of MitoTracker Red CMXRos staining and the quantitative analysis of mitochondrial length (magnification = 400 ×; 80–100 mitochondria were selected for analysis, n = 3). (E) Representative transmission electron microscopy (TEM) images of cells (magnification = 7,000 ×; 20–30 mitochondria were selected for analysis, n = 3), and the quantitative analysis of the length and area of mitochondria. Experimental data are expressed as the mean ± standard error of mean (SEM), n = 3. **P < 0.01 vs. Control group, and #P < 0.05 and ###P < 0.01 vs. Aβ₄₂ group. Mdivi1: mitochondrial division inhibitor 1.

target the root causes. In the context of neurodegenerative disorders, such as AD, the precise regulation of mitophagy and mitochondrial dynamics plays an essential role in maintaining cellular health. By meticulously examining these intricate biological processes, we aimed to elucidate the potential roles of DZSM in modulating these processes and discern how they contribute to the enhancement of cognitive function, attenuation of neuronal loss, and restoration of normal synaptic functionality.

DZSM is a patented Chinese medicine that originates from the ancient Chinese herbal compound prescription Shengmai san, which

was invented by Yuansu Zhang, a famous doctor who lived during the Jin Dynasty. This compound has been extensively used for the treatment of cardiovascular and cerebrovascular diseases in the clinic. Due to its effectiveness, DZSM has also been widely used by clinicians to treat AD. However, the complexity of the active ingredients of DZSM significantly limits its application and popularity. To further investigate the therapeutic effects of DZSM on AD, MRI and UPLC-MS/MS were used to analyse the brain regions of AD rats which DZSM acted on and the active components of DZSM, respectively. We found that several active components of DZSM can penetrate the blood-

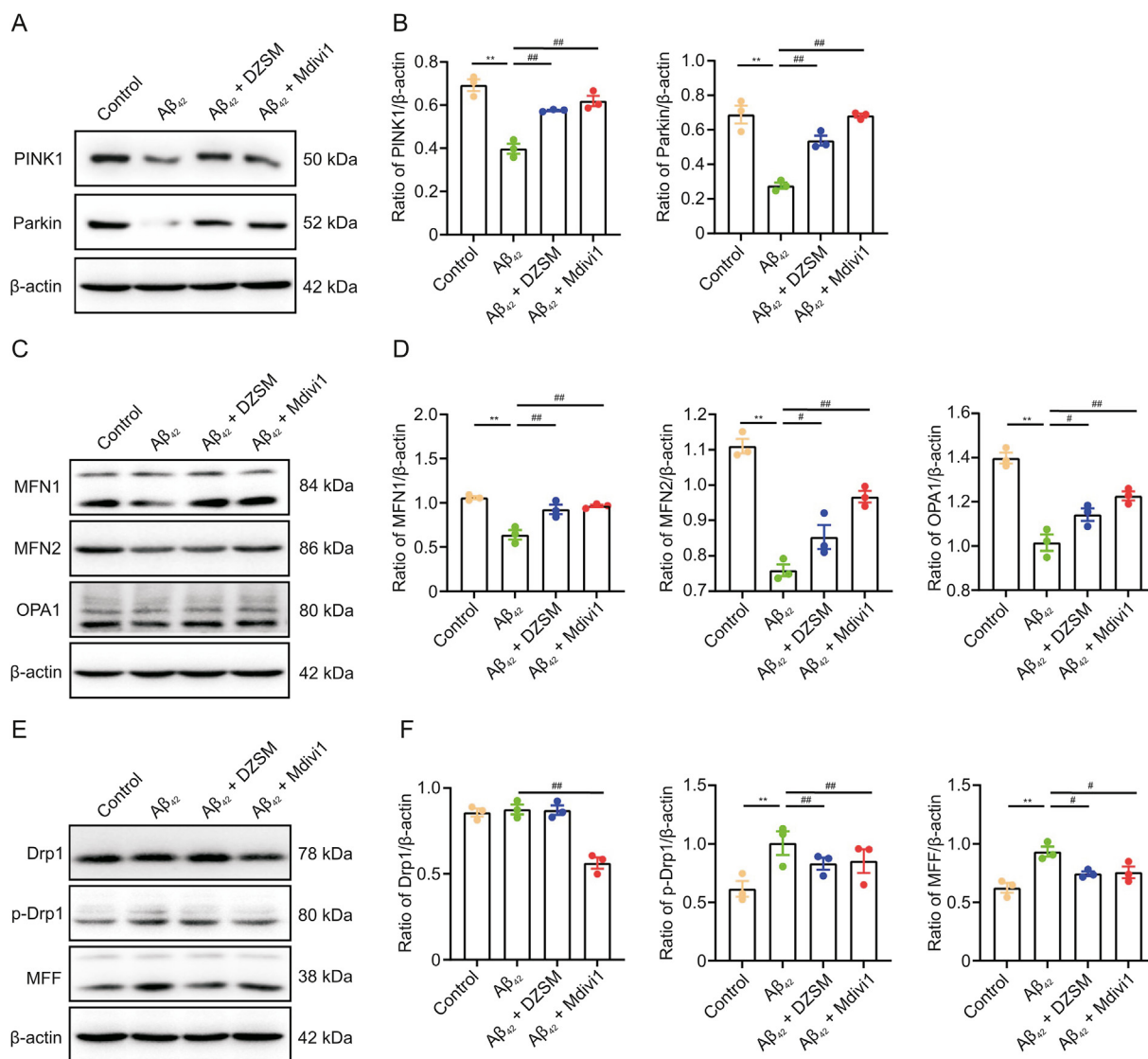


Fig. 10. Dengzhan Shengmai (DZSM) alleviates A β_{42} -induced mitochondrial dysfunction and fragmentation by regulating mitophagy and Drp1-mediated mitochondrial fission. (A) Representative protein electrophoresis bands for PINK1 and Parkin in various groups of cells. (B) Quantitative analysis of the protein expression levels of PINK1 and Parkin ($n = 3$). (C) Representative protein electrophoresis bands for MFN1, MFN2, and OPA1 in various groups of cells. (D) Quantitative analysis of the protein expression levels of MFN1, MFN2, and OPA1 in cells ($n = 3$). (E) Representative protein electrophoresis bands for Drp1, p-Drp1, and MFF in various groups of cells. (F) Quantitative analysis of the protein expression levels of Drp1, p-Drp1, and MFF in cells ($n = 3$). Experimental data are expressed as the mean \pm standard error of mean (SEM), $n = 3$. ** $P < 0.01$ vs. Control group, and * $P < 0.05$ and ## $P < 0.01$ vs. A β_{42} group. Mdivi1: mitochondrial division inhibitor 1.

brain barrier. DZSM ameliorates hippocampal structural damage in AD model rats. These results demonstrated that the hippocampus is an important brain region targeted by DZSM for treatment of AD.

In this study, simultaneous establishment encompassed not only the AD + DZSM group, but also the DZSM group. The inclusion of DZSM group in our study had two-fold significance. First, it functioned as a crucial control/reference group, enabling isolation of DZSM's direct effects on synaptic currents, mitophagy, and mitochondrial dynamics from those influenced by AD pathology. This distinction aided in unveiling the unique contributions of DZSM to cellular processes and refined our understanding of its therapeutic potential. Second, the DZSM group provided insights into the broader physiological implications of DZSM administration, establishing a baseline for normal responses and enhancing the robustness of our findings. By meticulously considering DZSM's impact on normal conditions, this group enriched our conclusions

and ensured a comprehensive interpretation of outcomes in the context of AD and DZSM intervention.

Synaptic damage and A β deposition are important pathological features of AD. Previous studies have demonstrated that lateral ventricle injection of A β_{42} induces synaptic damage in the rat hippocampus [50–52] and loss of hippocampal neurons in rodents [27,53]. In this study, the primary neuronal cells induced by A β_{42} were used as *in vitro* experiment models. ATP detection, MMP and ROS examination, mitochondrial morphology analysis, electrophysiological studies, and Western blotting were performed to verify the effects and molecular mechanisms of DZSM on synaptic and mitochondrial dysfunction. The results indicated that DZSM can alleviate A β_{42} -induced mitochondrial dysfunction and fragmentation by regulating mitophagy and Drp1-mediated mitochondrial fission. Taken together, DZSM was proved to alleviate cognitive impairment by modulating mitophagy and mitochondrial

fusion and fission along with energy metabolism in A β ₁₋₄₂ induced AD animal and cellular models.

SPs are important pathological features of AD. The formation of SPs is related to the accumulation of extracellular A β [54]. Previous studies have shown that injections of A β ₄₂ in the lateral ventricle induces the formation of SPs in rodents [55–57]. Therefore, we established an AD rat model using A β ₄₂ and examined SPs in the hippocampus using thioflavin S staining. These results demonstrated that AD rats had significant SP deposition, whereas DZSM reduced the number of SPs in the hippocampus. A large number of studies have demonstrated that SPs are mainly composed of A β ₄₀ and A β ₄₂ [58–60]. In this study, we examined the expression levels of insoluble/soluble A β ₄₀ and insoluble/soluble A β ₄₂ in the hippocampus using ELISA. The results demonstrated that the expression levels of insoluble/soluble A β ₄₀ and insoluble/soluble A β ₄₂ were significantly elevated in the hippocampus of AD rats, whereas DZSM reversed the phenomenon. A β production is related to α -secretase (ADAM10), BACE1, PS1 and IDE [61,62]. Therefore, we examined the expression levels of these proteins in the hippocampus using Western blotting. DZSM increased the level of IDE in the hippocampus but had no significant effect on the expression levels of ADAM10, BACE1, and PS1. The aforementioned results strongly suggest that DZSM reduced SP deposition in the hippocampus by increasing related A β -degrading enzymes.

Neurons and synapses are the biological basis of hippocampus-dependent learning and memory. A β is extremely cytotoxic. It induces neuronal loss and synaptic damage, resulting in the impairment of hippocampus-dependent learning and memory [63,64]. In this study, we performed Nissl staining to label neurons in the hippocampal regions, in an attempt to determine whether DZSM alleviated A β -induced neuronal loss. The results indicated that DZSM increased the number of neurons in the hippocampus, suggesting that DZSM inhibited A β -induced neuronal loss in the hippocampus. To determine whether DZSM alleviated A β -induced synaptic damage, we examined the ultrastructure of hippocampal synapses, the density and length of dendritic spines, and dendritic branching using TEM and Golgi staining. DZSM increased the length and width of postsynaptic density, density and length of dendritic spines, and dendritic branching in the hippocampus. These findings indicate that DZSM alleviated A β -induced synaptic damage. In addition, we examined the expression levels of synaptic marker proteins (PSD95 and SYN1) in the hippocampus using immunofluorescence and western blotting. Our results showed that DZSM increased the expression of PSD95 and SYN1 in the hippocampus. Electrophysiological data also confirmed the modulatory effects on synaptic transmissions. These results demonstrated that DZSM alleviated A β -induced neuronal loss and synaptic damage. We found that DZSM-containing serum increased the expression levels of PSD95 and SYN1 in the AD cell model.

These results demonstrate the protective effects of DZSM on neurons and synapses. To further reveal the molecular mechanisms by which DZSM improves AD, TMT label-based proteomics were used to identify the altered proteins in the hippocampi of AD rats. The components entering the brain were identified using UPLC-MS/MS analysis. By combining the results of proteomics and enrichment analyses, the key role of energy metabolism was identified as the focus of follow-up studies.

Mitochondria are the metabolic centres and energy factories of cells. They play a decisive role in determining the fate of the cell. Neurons are highly differentiated mitotic cells with high energy demand [11]. Therefore, neurons are inherently dependent on mitochondrial function [65]. Mitochondria are highly sensitive to A β , which can damage their structure and function. Previous studies have also demonstrated that mitochondrial dysfunction is

an important pathological manifestation of AD and that the occurrence of mitochondrial dysfunction precedes the formation of SP and neurofibrillary tangles [13–15].

Hippocampal proteomic analysis was conducted to elucidate the effects of DZSM intervention on AD. The observed differential protein expression between the AD and DZSM groups revealed the potential impact of DZSM intervention on multiple biological processes in the hippocampus. The enrichment of proteins associated with synaptic chemical transmission, mitochondrial function, and energy metabolism aligned with our previous findings on altered synaptic currents and mitochondrial dynamics in AD rats. Importantly, the notable influence of DZSM on biological processes such as mitochondrial respiratory chain complex I assembly, glycolytic processes, and ATP hydrolysis-coupled proton transport suggests a potential role of DZSM in enhancing energy metabolism and mitochondrial function. The molecular functions attributed to the differentially expressed proteins, including protein binding, poly(A) RNA binding, and calmodulin binding, further emphasised the multifaceted interactions that contribute to the therapeutic effects of DZSM. This aligns with the complexity of neuronal signalling and maintenance processes.

The KEGG analysis outcomes underscored the relevance of DZSM intervention in mitigating neurodegenerative diseases. The enrichment of pathways associated with Huntington's disease, AD, and PD indicated the potential of DZSM in modulating common mechanisms shared among these conditions. Moreover, the involvement of metabolic pathways, oxidative phosphorylation, and other energy-related processes aligned with our hypothesis regarding the influence of DZSM on mitochondrial function. The correlation between the proteomics results and our earlier observations regarding synaptic improvements, cognitive protection, and mitochondrial dynamics further strengthens our hypothesis that the therapeutic effects of DZSM on AD may be linked to its ability to restore mitochondrial health and energy metabolism. Collectively, these findings provide a comprehensive molecular foundation for the positive outcomes observed with DZSM intervention.

Proteomic analysis revealed intricate connections between DZSM intervention and hippocampal proteomics. These findings collectively support our hypothesis that the effect of DZSM on mitochondrial function and energy metabolism underlies its therapeutic potential for ameliorating AD-related changes. Further investigations on specific protein interactions and pathways will undoubtedly provide more nuanced insights into the precise mechanisms by which DZSM exerts its beneficial effects, which would lay a solid foundation for subsequent critical investigations of mitophagy and mitochondrial dynamics in the context of AD.

In this study, both animal and cellular experiments confirmed that DZSM increased the expression level of ATP in the rat hippocampus and primary cells. Previous studies have shown that A β ₄₂ induces mitochondrial dysfunction in primary neural cells and SH-SY5Y cells [39,66]. In this study, the *in vivo* experiments demonstrated that DZSM increased MMP in primary cells and decreased ROS content in the hippocampus. These results confirmed that DZSM improved A β -induced mitochondrial dysfunction. Therefore, we further evaluated the effects of DZSM on A β ₄₂-induced mitochondrial dysfunction in primary neural cells *in vitro*. Under physiological conditions, 90% of cellular ROS are produced by mitochondria. Mitochondrial dysfunction accelerates ROS production and causes ROS accumulation in cells [67].

Interestingly, we found that the length of mitochondria was significantly reduced in AD rats and the AD cell model in comparison to the control group, indicating that A β induced mitochondrial fragmentation. Further investigation revealed that the expression

levels of mitochondrial fusion proteins (MFN1, MFN2, and OPA1) were downregulated and those of mitochondrial fission proteins (MFF and phosphorylated Drp1) were upregulated in AD rats and the AD cell model. These results suggest that mitochondrial fragmentation may be related to an imbalance in mitochondrial dynamics [68,69]. Previous studies have shown that mitochondria meets the energy demands of neurons in different states through continuous fusion and fission [70,71]. An imbalance in mitochondrial fusion/fission may lead to mitochondrial dysfunction and fragmentation. In the present study, DZSM increased the expression of MFN1, MFN2, and OPA1 in the hippocampi of AD rats. Moreover, DZSM inhibited the expression of MFF and phosphorylated Drp1 in the hippocampus. These results indicate that DZSM improved A β -induced mitochondrial dysfunction and fragmentation by regulating mitochondrial fusion/fission.

In recent years, studies have demonstrated that A β induces mitochondrial structural and functional damage in AD, and also causes mitophagy defects. Mitophagy eliminates damaged mitochondria and is important for maintaining mitochondrial function. This study demonstrated that DZSM alleviated mitochondrial dysfunction and fragmentation in AD, both *in vivo* and *in vitro*. Therefore, we further investigated the molecular mechanisms *in vitro* through which DZSM improves mitochondrial dysfunction and fragmentation in AD. Under physiological conditions, balanced mitochondrial function is maintained by the regulation of mitophagy, mitochondrial biogenesis, and mitochondrial fusion and fission. Moreover, mitochondrial function adapts to the energy needs of cells [17]. However, defects in mitophagy and a dynamic imbalance between mitochondrial fusion and fission leads to mitochondrial dysfunction [72]. The PINK1/Parkin pathway is a key pathway that regulates mitophagy, and the activation of this signalling pathway alleviates mitochondrial dysfunction and synaptic damage in AD [73–75]. Mitochondrial fusion and fission are crucial for maintaining mitochondrial structure and function. Previous studies have demonstrated that Drp1 is a key regulator of mitochondrial fission. Phosphorylation of Drp1 at Ser616 increases mitochondrial fission, and causes mitochondrial dysfunction and fragmentation [70,71]. Mdivi1 is a small molecule inhibitor of Drp1. Studies have shown that Mdivi1 inhibits phosphorylation of Drp1 at Ser616 by reducing Drp1 activity, thereby alleviating mitochondrial dysfunction and fragmentation [20,48].

Drp1 is a key protein that regulates mitochondrial fission. Inhibition of Drp1 reportedly improves mitochondrial dysfunction and fragmentation in AD [20,48]. To further explore the molecular mechanism by which DZSM improved mitochondrial dysfunction, this study established an AD cell model using A β_{42} and treated the model with DZSM-containing serum and Mdivi1. The results showed that DZSM-containing serum increased the expression of MFN1, MFN2, and OPA1, and inhibited the expression of phosphorylated Drp1 and MFF. These results confirmed that DZSM improved A β -induced mitochondrial dysfunction and fragmentation by inhibiting Drp1-mediated mitochondrial fission.

In recent years, certain studies have shown that mitophagy is deficient in patients with AD and that activation of mitophagy improves mitochondrial dysfunction. The activation of mitophagy-related proteins, such as PTEN-induced kinase 1 (PINK1) and Parkin, reportedly improves mitochondrial dysfunction in AD [73–75]. This study found that DZSM increased the expression of the mitophagy proteins, PINK1 and Parkin, in AD rats and an AD cell model. These findings indicate that DZSM improved A β -induced mitochondrial dysfunction by activating mitophagy.

This study had some limitations. We did not use different doses of DZSM or a positive control such as donepezil hydrochloride. DZSM has long been used in clinical treatments and has shown promising results and safety profiles. The administered dosage for

rats was converted according to the human clinical dosage. This study aimed to elucidate the pharmacological mechanisms of DZSM. Moreover, this study could not completely determine the specific active ingredients of DZSM that provided the therapeutic effect, which will be the goal of our next study.

5. Conclusion

In summary, this study established a cohesive narrative linking the intricate interplay of altered synaptic currents, mitophagy, and mitochondrial dynamics in AD pathology. These results demonstrated that DZSM improved mitochondrial dysfunction by activating mitophagy and inhibiting Drp1-mediated mitochondrial fission, thereby alleviating neuronal loss and synaptic dysfunction in AD rat model and primary neural cells. The synergy between the exploration of these molecular intricacies and the therapeutic potential of DZSM underscores the integrated nature of this study, paving the way for a more comprehensive understanding of the complex pathogenesis of AD and the potential for innovative therapeutic interventions.

CRediT author statement

Binbin Zhao, and **Dongfeng Wei**: Conceptualization, Investigation, Formal analysis, Writing - Original draft preparation; **Qinghua Long**, **Qingjie Chen**, and **Fushun Wang**: Methodology, Writing - Reviewing and Editing; **Linlin Chen**, **Zefei Li**, **Tong Li**, **Tao Ma**, and **Wei Liu**: Investigation, Writing - Reviewing and Editing; **Linshuang Wang**: Visualization; **Caishui Yang**, and **Xiaxia Zhang**: Formal analysis, Data curation; **Ping Wang**, and **Zhanjun Zhang**: Supervision, Funding acquisition, Project administration.

Declaration of competing interest

The authors declare that there are no conflicts of interest.

Acknowledgments

This work was supported by National Natural Science Foundation of China (Grant No.: 82374317), State Key Program of National Natural Science of China (Grant Nos.: 82130119 and 82130118), Postdoctoral Research Foundation of China (Grant No.: 2021M690450), Traditional Chinese Medicine Research Project of Health Commission of Hubei Province (Grant No.: ZY2021M017), Hubei University of Chinese Medicine Funds for Distinguished Young Scholars (Grant No.: 2022ZZXJ004), National Natural Science Foundation of China (Grant No.: 82174210), and Fundamental Research Funds for the Central Public Welfare Research Institutes (Grant No.: ZZ14-FL-005).

Appendix A. Supplementary data

Supplementary data to this article can be found online at <https://doi.org/10.1016/j.jpha.2023.10.006>.

References

- [1] L. Jia, Y. Du, L. Chu, et al., Prevalence, risk factors, and management of dementia and mild cognitive impairment in adults aged 60 years or older in China: A cross-sectional study, *Lancet Public Health* 5 (2020) e661–e671.
- [2] J. Jia, C. Wei, S. Chen, et al., The cost of Alzheimer's disease in China and re-estimation of costs worldwide, *Alzheimers Dement.* 14 (2018) 483–491.
- [3] S. Park, H.Y. Kim, H.A. Oh, et al., Quinacrine directly dissociates amyloid plaques in the brain of 5XFAD transgenic mouse model of Alzheimer's disease, *Sci. Rep.* 11 (2021), 12043.

- [4] Y. Deng, Z. Xiong, P. Chen, et al., β -amyloid impairs the regulation of N-methyl-D-aspartate receptors by glycogen synthase kinase 3, *Neurobiol. Aging* 35 (2014) 449–459.
- [5] A.V. Blagov, A.V. Grechko, N.G. Nikiforov, et al., Role of impaired mitochondrial dynamics processes in the pathogenesis of Alzheimer's disease, *Int. J. Mol. Sci.* 23 (2022), 6954.
- [6] K. Panchal, A.K. Tiwari, Mitochondrial dynamics, a key executioner in neurodegenerative diseases, *Mitochondrion* 47 (2019) 151–173.
- [7] T.O. Tobore, On the etiopathogenesis and pathophysiology of Alzheimer's disease: A comprehensive theoretical review, *J. Alzheimers Dis.* 68 (2019) 417–437.
- [8] A. Serrano-Pozo, S. Das, B.T. Hyman, APOE and Alzheimer's disease: Advances in genetics, pathophysiology, and therapeutic approaches, *Lancet Neurol.* 20 (2021) 68–80.
- [9] M. Calvo-Rodriguez, B.J. Bacskaï, Mitochondria and calcium in Alzheimer's disease: From cell signaling to neuronal cell death, *Trends Neurosci.* 44 (2021) 136–151.
- [10] Z. Tian, Y. Zhang, Z. Zheng, et al., Gut microbiome dysbiosis contributes to abdominal aortic aneurysm by promoting neutrophil extracellular trap formation, *Cell Host Microbe* 30 (2022) 1450–1463.e8.
- [11] A. Grimm, A. Eckert, Brain aging and neurodegeneration: From a mitochondrial point of view, *J. Neurochem.* 143 (2017) 418–431.
- [12] X. Sui, R. Zhang, S. Liu, et al., RSL3 drives ferroptosis through GPX4 inactivation and ROS production in colorectal cancer, *Front. Pharmacol.* 9 (2018), 1371.
- [13] R.H. Swerdlow, J.M. Burns, S.M. Khan, The Alzheimer's disease mitochondrial cascade hypothesis: Progress and perspectives, *Biochim. Biophys. Acta* 1842 (2014) 1219–1231.
- [14] R.H. Swerdlow, S.M. Khan, A "mitochondrial cascade hypothesis" for sporadic Alzheimer's disease, *Med. Hypotheses* 63 (2004) 8–20.
- [15] P.H. Reddy, R. Tripathi, Q. Troung, et al., Abnormal mitochondrial dynamics and synaptic degeneration as early events in Alzheimer's disease: Implications to mitochondria-targeted antioxidant therapeutics, *Biochim. Biophys. Acta BBA Mol. Basis Dis.* 1822 (2012) 639–649.
- [16] J.M. Perez Ortiz, R.H. Swerdlow, Mitochondrial dysfunction in Alzheimer's disease: Role in pathogenesis and novel therapeutic opportunities, *Br. J. Pharmacol.* 176 (2019) 3489–3507.
- [17] W. Wang, F. Zhao, X. Ma, et al., Mitochondria dysfunction in the pathogenesis of Alzheimer's disease: Recent advances, *Mol. Neurodegener.* 15 (2020), 30.
- [18] H. Wang, J. Fu, X. Xu, et al., Rapamycin activates mitophagy and alleviates cognitive and synaptic plasticity deficits in a mouse model of Alzheimer's disease, *J. Gerontol A Biol Sci Med Sci* 76 (2021) 1707–1713.
- [19] Z.T. Wang, M.H. Lu, Y. Zhang, et al., Disrupted-in-schizophrenia-1 protects synaptic plasticity in a transgenic mouse model of Alzheimer's disease as a mitophagy receptor, *Aging Cell* 18 (2019), e12860.
- [20] A.F. Batista, T. Rody, L. Forný-Germano, et al., Interleukin-1 β mediates alterations in mitochondrial fusion/fission proteins and memory impairment induced by amyloid- β oligomers, *J. Neuroinflammation* 18 (2021), 54.
- [21] P. Huang, X.Y. He, M. Xu, Dengzhan Shengmai capsule combined with donepezil hydrochloride in the treatment of Alzheimer's disease: Preliminary findings, randomized and controlled clinical trial, *Rev. Assoc. Med. Bras.* (1992) 67 (2021) 190–194.
- [22] S. Zhang, J. Zhang, D. Wei, et al., Dengzhan Shengmai capsules and their active component scutellarin prevent cognitive decline in APP/PS1 mice by accelerating A β aggregation and reducing oligomers formation, *Biomed. Pharmacother.* 121 (2020), 109682.
- [23] H. Lu, J. Zhang, Y. Liang, et al., Network topology and machine learning analyses reveal microstructural white matter changes underlying Chinese medicine Dengzhan Shengmai treatment on patients with vascular cognitive impairment, *Pharmacol. Res.* 156 (2020), 104773.
- [24] N. Sheng, H. Zheng, M. Li, et al., 4,5-caffeoylquinic acid and scutellarin, identified by integrated metabolomics and proteomics approach as the active ingredients of Dengzhan Shengmai, act against chronic cerebral hypoperfusion by regulating glutamatergic and GABAergic synapses, *Pharmacol. Res.* 152 (2020), 104636.
- [25] L. Wang, Q. Ma, Clinical benefits and pharmacology of scutellarin: A comprehensive review, *Pharmacol. Ther.* 190 (2018) 105–127.
- [26] S. Zhang, P. Wang, L. Ren, et al., Protective effect of melatonin on soluble A β 1-42-induced memory impairment, astrogliosis, and synaptic dysfunction via the Musashi1/Notch1/Hes1 signaling pathway in the rat hippocampus, *Alzheimers Res. Ther.* 8 (2016), 40.
- [27] X. Jiang, L. Chen, Z. Lan, et al., Icaritin ameliorates amyloid pathologies by maintaining homeostasis of autophagic systems in A β 1-42-injected rats, *Neurochem. Res.* 44 (2019) 2708–2722.
- [28] J. McInnes, K. Wierda, A. Snellinx, et al., Synaptogyrin-3 mediates presynaptic dysfunction induced by tau, *Neuron* 97 (2018) 823–835.e8.
- [29] W.D. Bao, P. Pang, X.T. Zhou, et al., Loss of ferroptin induces memory impairment by promoting ferroptosis in Alzheimer's disease, *Cell Death Differ.* 28 (2021) 1548–1562.
- [30] D. Puzzo, L. Lee, A. Palmeri, et al., Behavioral assays with mouse models of Alzheimer's disease: Practical considerations and guidelines, *Biochem. Pharmacol.* 88 (2014) 450–467.
- [31] E.S. Lein, M.J. Hawrylycz, N. Ao, et al., Genome-wide atlas of gene expression in the adult mouse brain, *Nature* 445 (2007) 168–176.
- [32] N.S. Hübner, A.E. Mechling, H.L. Lee, et al., The connectomics of brain demyelination: Functional and structural patterns in the cuprizone mouse model, *NeuroImage* 146 (2017) 1–18.
- [33] S. Koch, S. Mueller, M. Foddis, et al., Atlas registration for edema-corrected MRI lesion volume in mouse stroke models, *J. Cereb. Blood Flow Metab.* 39 (2019) 313–323.
- [34] J.D. Tournier, R. Smith, D. Raffelt, et al., MRtrix3: A fast, flexible and open software framework for medical image processing and visualisation, *NeuroImage* 202 (2019), 116137.
- [35] J. Veraart, D.S. Novikov, D. Christiaens, et al., Denoising of diffusion MRI using random matrix theory, *NeuroImage* 142 (2016) 394–406.
- [36] M.S. Graham, I. Drobnjak, H. Zhang, Realistic simulation of artefacts in diffusion MRI for validating post-processing correction techniques, *NeuroImage* 125 (2016) 1079–1094.
- [37] B. Ding, C. Lin, Q. Liu, et al., Tanshinone IIA attenuates neuroinflammation via inhibiting RAGE/NF- κ B signaling pathway *in vivo* and *in vitro*, *J. Neuroinflammation* 17 (2020), 302.
- [38] D. Zhao, J. Meng, Y. Zhao, et al., RPS23RG1 is required for synaptic integrity and rescues Alzheimer's disease-associated cognitive deficits, *Biol. Psychiatry* 86 (2019) 171–184.
- [39] S.A. Farr, J.F. Scherrer, W.A. Banks, et al., Chronic ethanol consumption impairs learning and memory after cessation of ethanol, *Alcohol. Clin. Exp. Res.* 29 (2005) 971–982.
- [40] Y. Yang, Z. Wang, S. Jin, et al., Opposite monosynaptic scaling of BLP-vCA1 inputs governs hopefulness- and helplessness-modulated spatial learning and memory, *Nat. Commun.* 7 (2016), 11935.
- [41] B. Genç, M. Gautam, Ö. Gözütk, et al., Improving mitochondria and ER stability helps eliminate upper motor neuron degeneration that occurs due to mSOD1 toxicity and TDP-43 pathology, *Clin. Transl. Med.* 11 (2021), e336.
- [42] D.G. Jones, R.M. Devon, An ultrastructural study into the effects of pentobarbitone on synaptic organization, *Brain Res.* 147 (1978) 47–63.
- [43] Y. Tian, J. Lu, X. Hao, et al., FTH1 inhibits ferroptosis through ferritinophagy in the 6-OHDA model of Parkinson's disease, *Neurotherapeutics* 17 (2020) 1796–1812.
- [44] A.J. Valente, L.A. Maddalena, E.L. Robb, et al., A simple ImageJ macro tool for analyzing mitochondrial network morphology in mammalian cell culture, *Acta Histochem.* 119 (2017) 315–326.
- [45] F. Wang, N.A. Smith, Q. Xu, et al., Photolysis of caged Ca²⁺ but not receptor-mediated Ca²⁺ signaling triggers astrocytic glutamate release, *J. Neurosci.* 33 (2013) 17404–17412.
- [46] J. Park, J. Won, J. Seo, et al., Streptozotocin induces Alzheimer's disease-like pathology in hippocampal neuronal cells via CDK5/Drp1-mediated mitochondrial fragmentation, *Front. Cell. Neurosci.* 14 (2020), 235.
- [47] X. Wang, B. Su, H.G. Lee, et al., Impaired balance of mitochondrial fission and fusion in Alzheimer's disease, *J. Neurosci.* 29 (2009) 9090–9103.
- [48] J. Grohm, S.W. Kim, U. Mamrak, et al., Inhibition of Drp1 provides neuroprotection *in vitro* and *in vivo*, *Cell Death Differ.* 19 (2012) 1446–1458.
- [49] P. Yang, D. Sheng, Q. Guo, et al., Neuronal mitochondria-targeted micelles relieving oxidative stress for delayed progression of Alzheimer's disease, *Biomaterials* 238 (2020), 119844.
- [50] M. Hadipour, G.H. Meftahi, M.R. Afarinesh, et al., Crocin attenuates the granular cells damages on the dentate gyrus and pyramidal neurons in the CA3 regions of the hippocampus and frontal cortex in the rat model of Alzheimer's disease, *J. Chem. Neuroanat.* 113 (2021), 101837.
- [51] Z. Xia, W. Peng, S. Cheng, et al., Naoling Decoction restores cognitive function by inhibiting the neuroinflammatory network in a rat model of Alzheimer's disease, *Oncotarget* 8 (2017) 42648–42663.
- [52] S. Yang, H. Shi, P. Zeng, et al., Bushen-Huatan-Yizhi formula reduces spatial learning and memory challenges through inhibition of the GSK-3 β /CREB pathway in AD-like model rats, *Phytomedicine* 90 (2021), 153624.
- [53] L. Lin, S.S. Jadoon, S.Z. Liu, et al., Tanshinone IIA ameliorates spatial learning and memory deficits by inhibiting the activity of ERK and GSK-3 β , *J. Geriatr. Psychiatry Neurol.* 32 (2019) 152–163.
- [54] S.A. Rosales-Corral, D. Acuña-Castroviejo, A. Coto-Montes, et al., Alzheimer's disease: Pathological mechanisms and the beneficial role of melatonin, *J. Pineal Res.* 52 (2012) 167–202.
- [55] E. O'Hare, D.I.C. Scopes, E.M. Kim, et al., Novel 5-aryloxyppyrimidine SEN1576 as a candidate for the treatment of Alzheimer's disease, *Int. J. Neuropsychopharm.* 17 (2014) 117–126.
- [56] S. Shahidi, S.S. Asl, A. Komaki, et al., The effect of chronic stimulation of serotonin receptor type 7 on recognition, passive avoidance memory, hippocampal long-term potentiation, and neuronal apoptosis in the amyloid β protein treated rat, *Psychopharmacology* 235 (2018) 1513–1525.
- [57] S. Dai, J. Zhang, Y. Bao, et al., Intracerebroventricular injection of A β 1-42 combined with two-vessel occlusion accelerate Alzheimer's disease development in rats, *Pathol. Res. Pract.* 214 (2018) 1583–1595.
- [58] B.D.C. Boon, M. Bulik, A.J. Jonker, et al., The coarse-grained plaque: A divergent A β plaque-type in early-onset Alzheimer's disease, *Acta Neuropathol.* 140 (2020) 811–830.
- [59] S.J. Jung, S.H. Park, E.J. Lee, et al., Development of fluorescent probes that bind and stain amyloid plaques in Alzheimer's disease, *Arch. Pharmacol. Res.* 38 (2015) 1992–1998.
- [60] U. Ghosh, W.M. Yau, J. Collinge, et al., Structural differences in amyloid- β fibrils from brains of nondemented elderly individuals and Alzheimer's disease patients, *Proc. Natl. Acad. Sci. USA* 118 (2021), e2111863118.

- [61] S.J. Lee, E. Nam, H.J. Lee, et al., Towards an understanding of amyloid- β oligomers: Characterization, toxicity mechanisms, and inhibitors, *Chem. Soc. Rev.* 46 (2017) 310–323.
- [62] Y. Li, J. Zhang, J. Wan, et al., Melatonin regulates A β production/clearance balance and A β neurotoxicity: A potential therapeutic molecule for Alzheimer's disease, *Biomed. Pharmacother.* 132 (2020), 110887.
- [63] S. Tu, S.I. Okamoto, S.A. Lipton, et al., Oligomeric A β -induced synaptic dysfunction in Alzheimer's disease, *Mol. Neurodegener.* 9 (2014), 48.
- [64] Y.N. Jang, H. Jang, G.H. Kim, et al., RAPGEF2 mediates oligomeric A β -induced synaptic loss and cognitive dysfunction in the 3xTg-AD mouse model of Alzheimer's disease, *Neuropathol. Appl. Neurobiol.* 47 (2021) 625–639.
- [65] Y. Zhu, R. Huang, Z. Wu, et al., Deep learning-based predictive identification of neural stem cell differentiation, *Nat. Commun.* 12 (2021), 2614.
- [66] C. Zhao, P. Su, C. Lv, et al., Berberine alleviates amyloid β -induced mitochondrial dysfunction and synaptic loss, *Oxid. Med. Cell. Longev.* 2019 (2019) 1–11.
- [67] T. Yan, Y. Zhao, Acetaldehyde induces phosphorylation of dynamin-related protein 1 and mitochondrial dysfunction via elevating intracellular ROS and Ca²⁺ levels, *Redox Biol.* 28 (2020), 101381.
- [68] X.H. Zhou, W.X. Peng, S.L. Pan, et al., High glucose suppresses osteogenic differentiation and induces mitochondrial dysfunction in osteoblasts via SIRT1/RECQL4 Axis: A Laboratory study using mouse cells, *J. Biol. Reg. Homeos. Ag.* 36 (2022) 889–899.
- [69] X. Qin, K. Zhang, Y. Fan, et al., The bacterial MtrAB two-component system regulates the cell wall homeostasis responding to environmental alkaline stress, *Microbiol. Spectr.* 10 (2022), e0231122.
- [70] D.C. Chan, Mitochondrial dynamics and its involvement in disease, *Annu. Rev. Pathol.* 15 (2020) 235–259.
- [71] A.M. Bertholet, T. Delerue, A.M. Millet, et al., Mitochondrial fusion/fission dynamics in neurodegeneration and neuronal plasticity, *Neurobiol. Dis.* 90 (2016) 3–19.
- [72] H.B. Suliman, C.A. Piantadosi, Mitochondrial quality control as a therapeutic target, *Pharmacol. Rev.* 68 (2016) 20–48.
- [73] L. Vaillant-Beuchot, A. Mary, R. Pardossi-Piquard, et al., Accumulation of amyloid precursor protein C-terminal fragments triggers mitochondrial structure, function, and mitophagy defects in Alzheimer's disease models and human brains, *Acta Neuropathol.* 141 (2021) 39–65.
- [74] E.F. Fang, Y. Hou, K. Palikaras, et al., Mitophagy inhibits amyloid- β and tau pathology and reverses cognitive deficits in models of Alzheimer's disease, *Nat. Neurosci.* 22 (2019) 401–412.
- [75] A.P. Reddy, N. Sawant, H. Morton, et al., Selective serotonin reuptake inhibitor citalopram ameliorates cognitive decline and protects against amyloid beta-induced mitochondrial dynamics, biogenesis, autophagy, mitophagy and synaptic toxicities in a mouse model of Alzheimer's disease, *Hum. Mol. Genet.* 30 (2021) 789–810.